https://ntrs.nasa.gov/search.jsp?R=19830004033 2020-03-21T06:43:19+00:00Z

148000-1-F

Final Report

SP MOUNTAIN DATA ANALYSIS

R. F. RAWSON, R. E. HAMILTON, C. L. LISKOW
A. R. DIAS, and P. L. JACKSON
Radar and Optics Division

SEPTEMBER 1981

National Aeronautics and Space Administration
Johnson Space Center
Houston, Texas 77058

Contract No. NAG 9-1-79-189 (R1)

ENVIRONMENTAL
RESEARCH INSTITUTE OF MICHIGAN
BOX 8618 • ANN ARBOR • MICHIGAN 48107

TECHNICAL REPORT STANDARD TITLE PAGE

1. Report No.	2. Government Accession No.	3. Recipient's Catalog No.

4. Title and Subtitle	5. Report Date
SP Mountain Data Analysis	September 1981
	6. Performing Organization Code
7. Author(s) R.F. Rawson, R.E. Hamilton, C.L. Liskow, A.R. Dias, and P.L. Jackson	8. Performing Organization Report No. 148000-1-F
9. Performing Organization Name and Address Environmental Research Institute of Michigan Radar and Optics Division P.O. Box 8618 Ann Arbor, Michigan 48107	10. Work Unit No.
	11. Contract or Grant No. NAG 9-1-79-189 (R1)
12. Sponsoring Agency Name and Address National Aeronautics and Space Administration Johnson Space Center Houston, Texas 77058	13. Type of Report and Period Covered Final Report 11 January 1980 through 10 September 1981
	14. Sponsoring Agency Code

15. Supplementary Notes

16. Abstract

An analysis of synthetic aperture radar data of SP Mountain was undertaken to demonstrate the use of digital image processing techniques to aid in geologic interpretation of SAR data. These data were collected with the ERIM X- and L-band airborne SAR using like- and cross-polarizations. The resulting signal films were used to produce computer compatible tapes, from which four-channel imagery was generated. Slant range-to-ground range and range-azimuth-scale corrections were made in order to facilitate image registration; intensity corrections were also made. Manual interpretation of the imagery showed that L-band represented the geology of the area better than X-band. Several differences between the various images were also noted. Further digital analysis of the corrected data was done for enhancement purposes. This analysis included application of an MSS differencing routine and development of a routine for removal of relief displacement. It was found that accurate registration of the SAR channels is critical to the effectiveness of the differencing routine. Use of the relief displacement algorithm on the SP Mountain data demonstrated the feasibility of the technique. Need for additional development of accurate registration and relief displacement algorithms is indicated.

17. Key Words	18. Distribution Statement
Synthetic aperture radar X- and L-band Parallel and cross polarization Radar imagery Digitization (Over)	

19. Security Classif. (of this report)	20. Security Classif. (of this page)	21. No. of Pages	22. Price
Unclassified		ix + 72	

17. Key Words (concluded)

Image registration
Intensity correction
Imagery interpretation
Differencing
Relief displacement

Page intentionally left blank

Page intentionally left blank

FOREWORD

The research results reported here were prepared for the National Aeronautics and Space Administration, Johnson Space Center (NASA, JSC) under a grant to the Environmental Research Institute of Michigan (ERIM), Radar and Optics Division. The technical monitor for NASA, JSC was Dr. M. B. Duke. Dr. P.L. Jackson* was Principal Investigator during the first 12 months of the program; Mr. R. F. Rawson was designated Principal Investigator for the completion of the program. R.E. Hamilton and C.L. Liskow provided analysis support and A.R. Dias provided support in using the ERIM digital processing facilities.

*Dr. Jackson is presently with the University of Michigan, Department of Geology, Ann Arbor, Michigan.

Page intentionally left blank

Page intentionally left blank

TABLE OF CONTENTS

Page intentionally left blank

Page intentionally left blank

LIST OF FIGURES

Page intentionally left blank

Page intentionally left blank

1
INTRODUCTION AND OBJECTIVES

1.1 INTRODUCTION

Data obtained with synthetic aperture radar (SAR) is processed to obtain imagery with intensity proportional to the reflectivity distribution of the scene imaged. During the past decade, and more, a large number of investigators have studied ways to model the observed reflectivity distribution in terms of physical surface properties for a variety of scattering surfaces. In order to validate models, measurements of the reflectivity of specific surfaces must be compared to the theoretical values of reflectivity as predicted by the models using ground measurements. In general practice, however, the extensive ground measurements of specific imaged sites needed to make these validations have been both difficult and expensive to obtain. Work on correlating the reflectivity distributions with physical surface parameters through scattering models has therefore been extremely limited.

The work described in this report has made use of available SAR data obtained at the SP Mountain lava flow. This particular site has been the subject of numerous investigations which have provided a wealth of scattering model information based on extensive ground measurements. The research reported here has taken advantage of both the SAR data collected by ERIM with the ERIM X-L SAR system, and the available model information, to correlate reflectivity distributions obtained from SAR data with the ground measurements and models describing the imaged area. The correlations were accomplished for 3 cm wavelength data (X-band) and 23 cm wavelength data (L-band). Both like (horizontal) and cross polarization data sets were utilized. Various image manipulations are required in order to fully utilize the SAR data for scattering studies. The availability of the X-L SAR data in particular has allowed the opportunity to demonstrate several sophisticated digital processing techniques.

1.2 OBJECTIVES

The research effort discussed in this report was carried out for the general purpose of analyzing existing X-L radar data of SP Mountain and its associated lava flow in such a way as to correlate the radar return with terrain surface roughness. In particular, the objectives of this analysis were to (1) analyze all four channels in terms of geological applications, (2) determine if the vegetation masks the geology, (3) apply Multispectral Scanner (MSS) enhancement techniques to the radar imagery, and (4) combine radar and MSS channels together.

The following chapters of this report discuss the steps taken toward meeting these objectives. Chapter 2 describes the data processing carried out to prepare the radar imagery for analysis and interpretation. Chapter 3 presents the results of manual interpretation of the imagery and discusses the digital image processing techniques applied to aid geologic interpretation. Chapter 4, the final chapter, presents the conclusions of the analysis and recommendations for further research in this area.

2
PREPARATION OF RADAR IMAGERY

This analysis made use of radar image data collected on 20 October 1979. During Pass 3 on that date, the SP Mountain area in Arizona was imaged by means of ERIM's X-L four-channel imaging radar mounted in a Canadian CV-580 aircraft. The flight altitude (i.e., height above ground) was approximately 15,000 ft and the antenna depression angle was 36°. The system used two transmitter channels, X-band and L-band, both at horizontal polarization. There were four receiver channels, two X-band and two L-band; for each wavelength, one channel received parallel-polarized signals and the other received cross-polarized signals*.

Signal data from the X-L SAR is recorded on film on-board the aircraft. Imagery is obtained from the signal data using a matched filter type processor in the ERIM optical processing facility. Two image formats can be obtained for analysis: (1) a film transparency and (2) digital data on a CCT. In this investigation, film transparencies of the imagery were utilized only to identify the test area to be used for further analysis. All subsequent data reduction was accomplished using the images in a CCT format.

This section describes, briefly, the steps in preparing the radar imagery for analysis. The preparations include the following steps: (1) digitization of the optically-processed imagery, (2) image generation and annotation, (3) image registration, (4) slant range-to-ground range coordinate transformation, (5) scale corrections, and (6) image intensity corrections. These various steps are described in this section.

*R.F. Rawson, F. Smith, and R. Larson, "The ERIM Simultaneous X- and L-Band Dual Polarization Radar", The Record of the IEEE 1975 International Radar Conference, 21-23 April 1975.

2.1 DIGITIZATION

The signal film which resulted from the data-collection mission was used as the input to ERIM's Hybrid Image Processing Facility (HIPF). This facility converted the analog image data to digital form and recorded the digital data on computer-compatible tape (CCT). Parameters of the digitization process are discussed in Appendix A. The resulting tapes, designated IPL 584, 585, 586, and 587, served as inputs to the data-analysis task discussed in this report.

2.2 IMAGERY GENERATION

The four (raw data) CCTs produced by HIPF were used by ERIM's Earth Resources Data Center (ERDC) to generate the uncorrected imagery shown in Figures 1a, 2a, 3a, and 4a. These radar images were all printed with north down in order to have the computer-printed identification oriented for easy reading.

Early in this program, it was decided that all imagery should be carefully labelled in order to avoid confusion. Therefore, a procedure was developed for placing pertinent information on each transparency along with the image. Using the CCT as its input, ERDC generated an image transparency upon which appears the header information plus certain letter codes which indicate the correction process applied to the data. All imagery presented in this report is so labelled.

2.3 IMAGE REGISTRATION

In order to compare the various radar-channel images with one another using a digital computer, it is necessary to register all four images. This registration requires a geometric reference, such as a topographic map, a satellite photo, or an appropriate aerial photo.

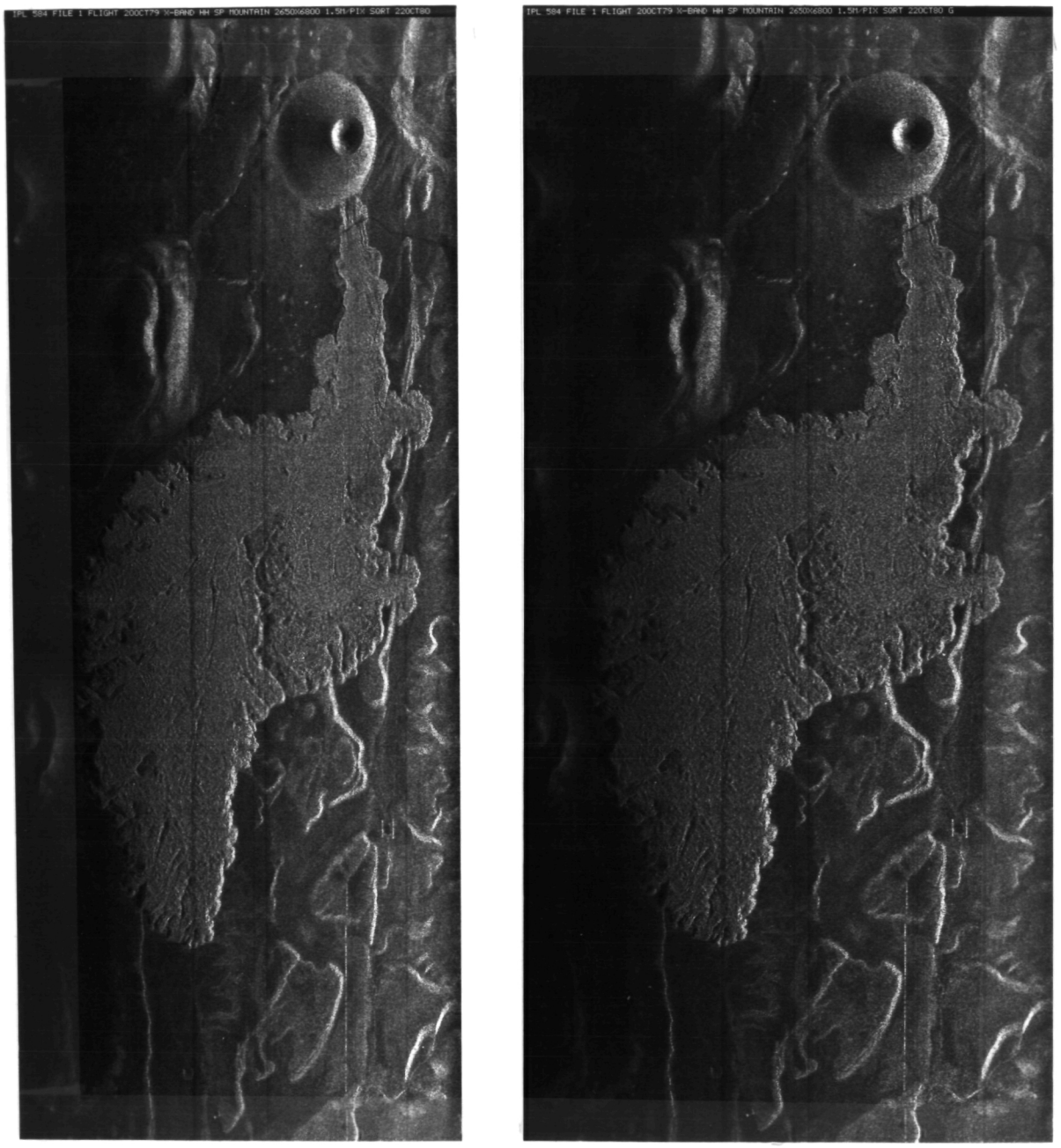

(a) Uncorrected

(b) SR-to-GR Corrected

FIGURE 1. ERDC IMAGERY, X-BAND, HH POLARIZATION.

.05-80
1.15-5

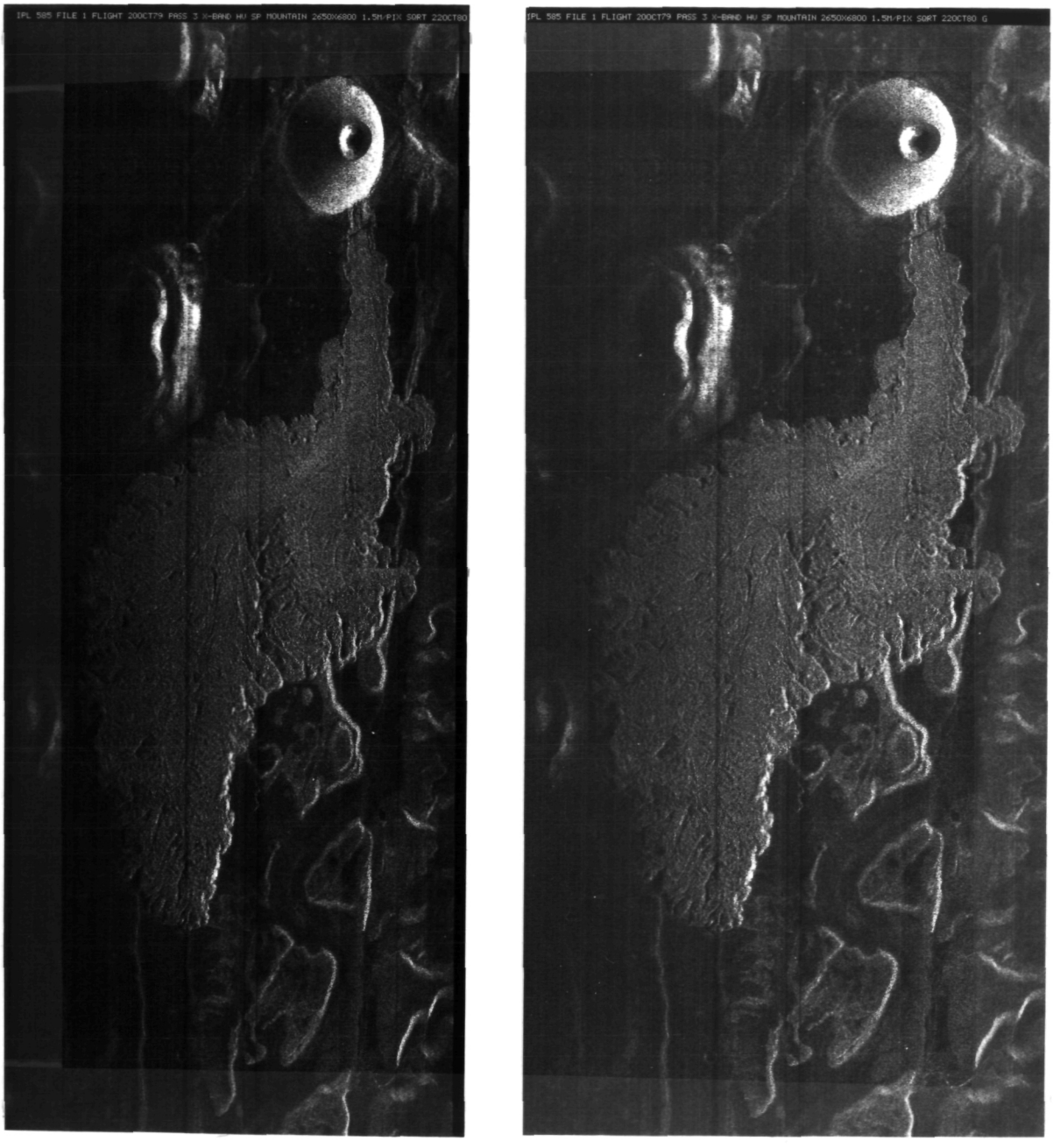

(a) Uncorrected

(b) SR-to-GR Corrected

FIGURE 2. ERDC IMAGERY, X-BAND, HV POLARIZATION.

·05-80
1-14-5

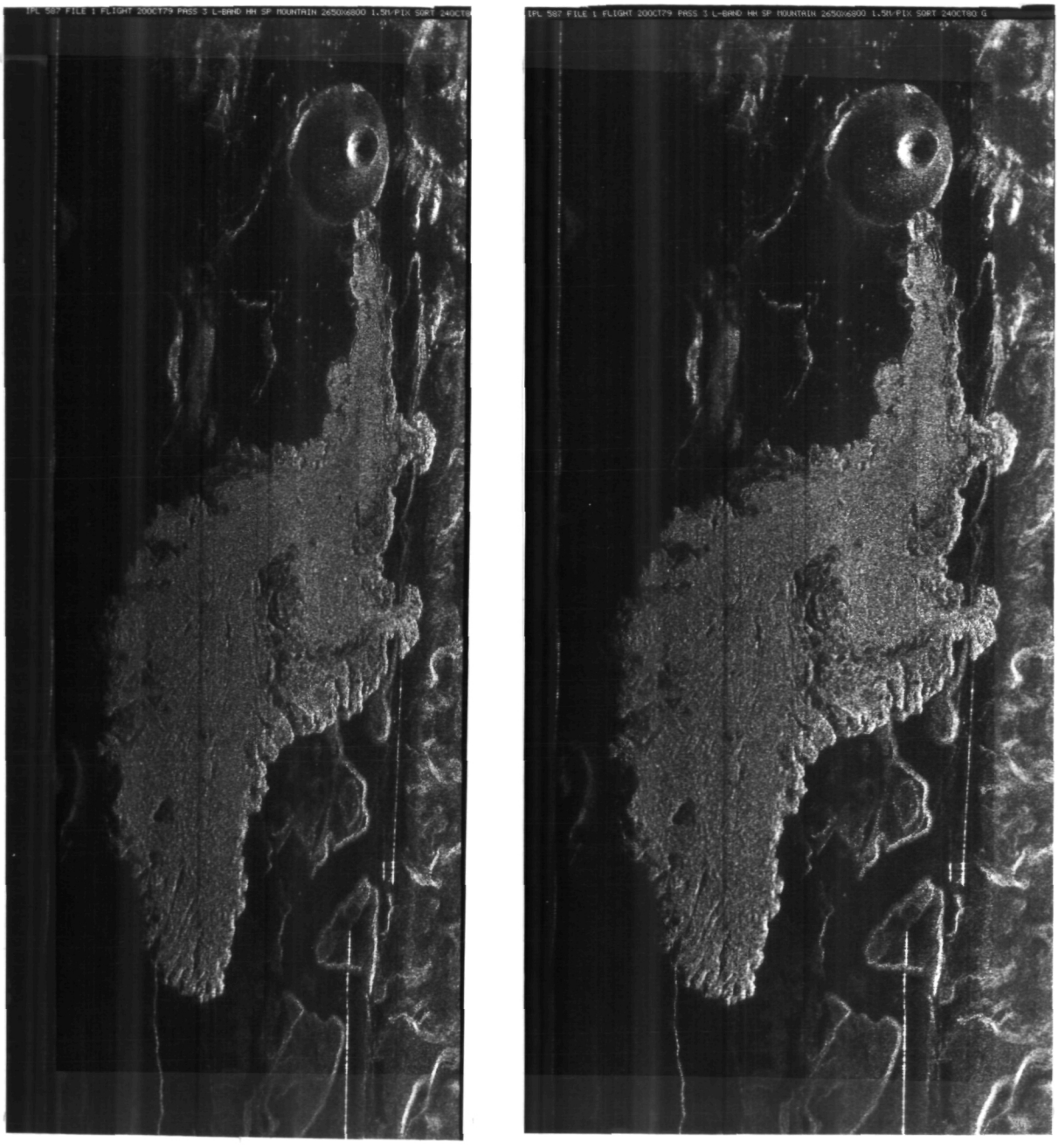

(a) Uncorrected

(b) SR-to-GR Corrected

FIGURE 3. ERDC IMAGERY, L-BAND, HH POLARIZATION.

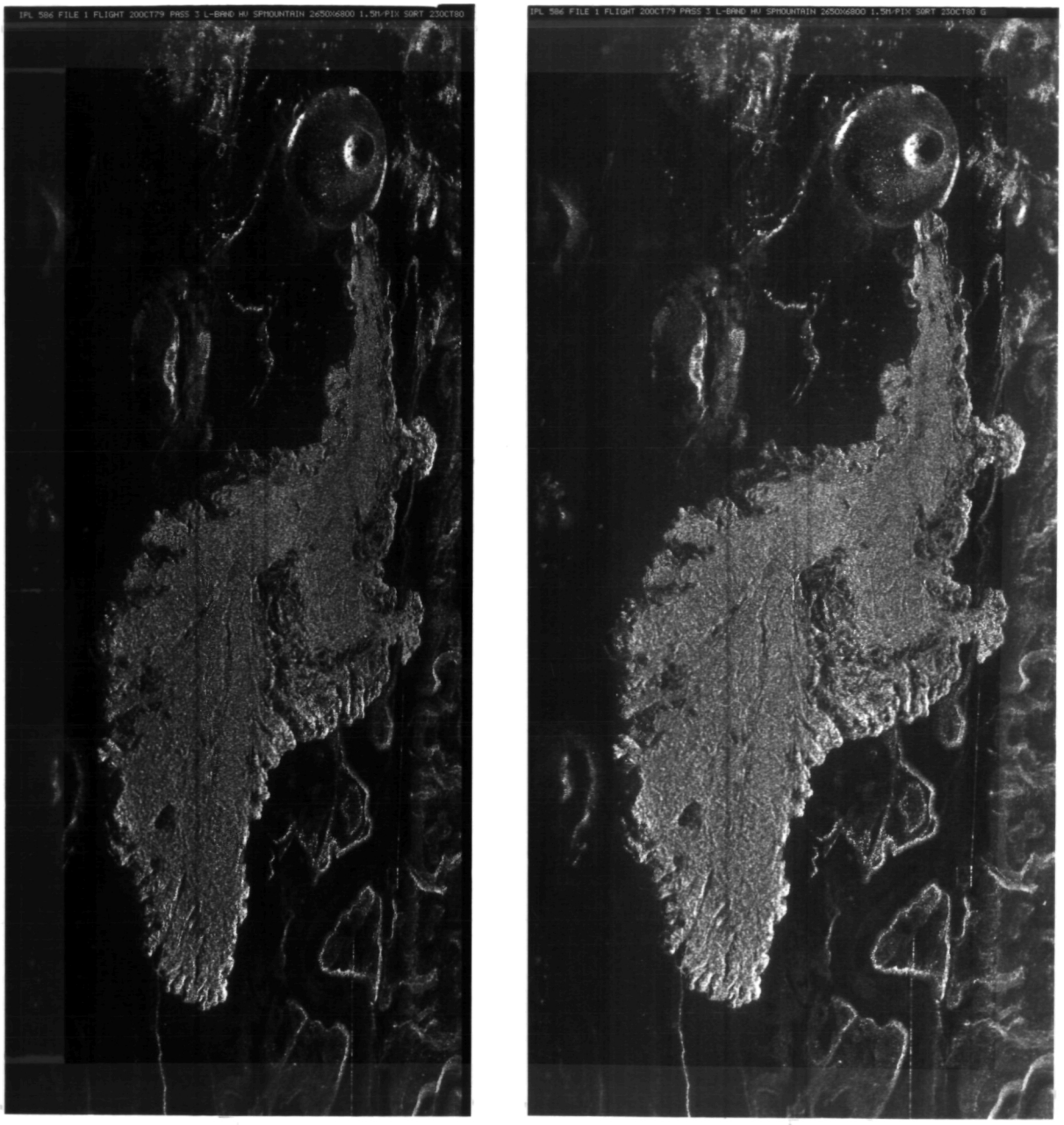

(a) Uncorrected

(b) SR-to-GR Corrected

FIGURE 4. ERDC IMAGERY, L-BAND, HV POLARIZATION.

.05 - 80
1.2 L - 7

For this program, registration was accomplished in the following manner. First, since the original digital radar image was linear in slant range, a conversion to ground-range coordinates was accomplished. Second, the range scale was adjusted with respect to the azimuth scale to obtain unity aspect ratio. These two steps were carried out in one operation using ERIM's Advanced Radar Imaging and Exploitation System (ARIES) digital computer facility and are described in the next two sections. Details of the digital computer work are presented in Appendix B.

2.3.1 SLANT-RANGE-TO-GROUND-RANGE CORRECTION

To accomplish the slant-range-to-ground-range (SR to GR) correction of the digital image data, an existing ERIM computer program was employed. This program employs a digital reconstruction filter to generate a new unequally-spaced set of data samples from the original samples which are equally spaced in slant range; Figure 5 illustrates the use of this filter. In order to effect the desired correction, the new samples must be unequally spaced in a very particular way, namely, such that they correspond to equal spacings in ground range. This is accomplished by considering the geometrical relationship between the slant range and ground range coordinate systems, as shown in Figure 6. From this figure, the following equation can be derived:

$$d_{sr} = \sqrt{d_{gr}^2 + h^2} - h \ , \qquad (1)$$

where d_{sr} is a slant-range distance, d_{gr} is the corresponding ground-range distance, and h is the aircraft's altitude above the terrain; these terms are clarified in Figure 6. Using this equation, equal ground range spacings Δd_{gr} will result in the proper unequal slant range spacings Δd_{sr}.

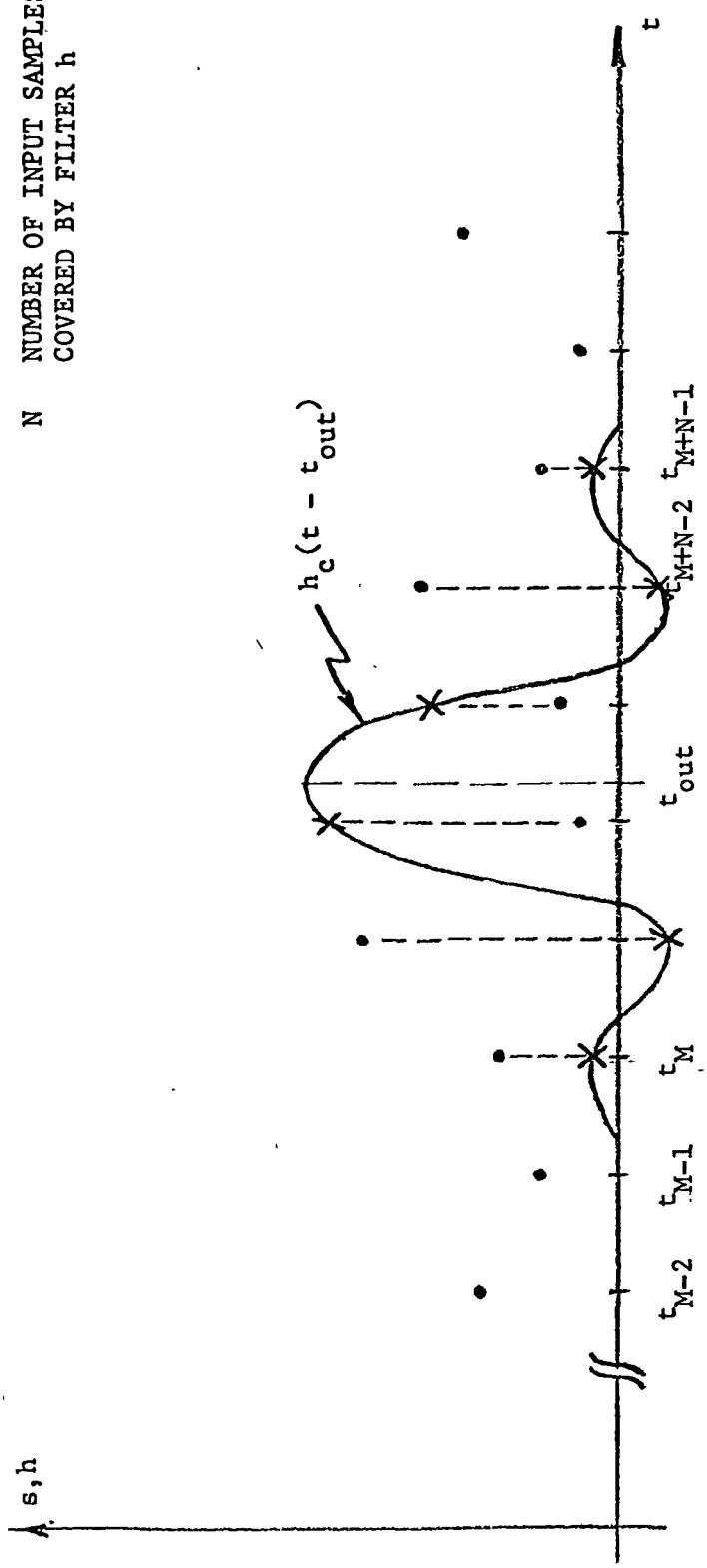

FIGURE 5. RECONSTRUCTION OF SLANT RANGE DATA.

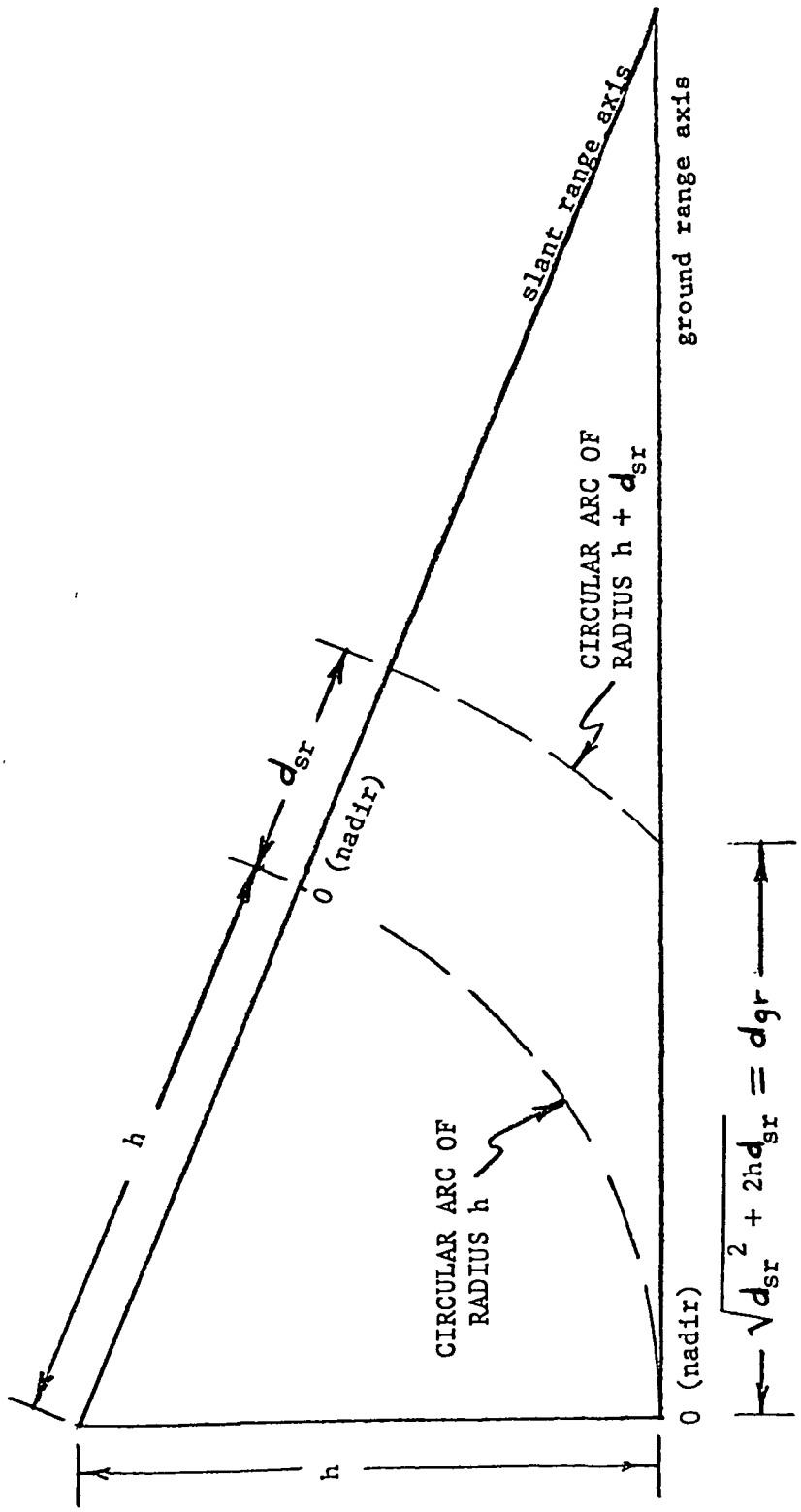

FIGURE 6. RELATIONSHIP BETWEEN SLANT RANGE AND GROUND RANGE COORDINATE SYSTEMS.

The imagery resulting from this SR-to-GR correction process is shown in Figures 1b, 2b, 3b, and 4b. Note that the code letter "G" (for "ground") has been appended to the header information to signify that this correction has been made.

2.3.2 RANGE-AZIMUTH SCALE CORRECTION

The original intent of this correction was that the range and azimuth scales on all four images be made equal. Unfortunately, this approach turned out to be very time-consuming and costly; it requires about eighteen hours of computer time per tape. An alternate approach was therefore selected which requires about one hour of computer time per tape; this approach corrects the ratio of the range and azimuth scales to unity, but does not make all four images exactly the same size. Further information about the two alternatives is given in Appendix B.

In order to determine the required correction factors, measurements were made on the SR-to-GR-corrected images in Figures 1b, 2b, 3b, and 4b. The procedure for determining the range-to-azimuth scale ratio was to first measure the range distance between two identifiable points spaced far apart in the radar image and to measure the corresponding distance on a satellite color photograph.* By dividing the former distance by the latter, a range quotient was calculated. Then, the same types of measurements were made in the azimuth direction and the corresponding azimuth quotient was formed. Finally, the range quotient was divided by the azimuth quotient to give the desired range-to-azimuth scale ratio. By simply inverting this ratio, the correction factor is obtained. Table 1 lists these factors for all four channels. It can be shown that these correction

*This reference was chosen because it was easier to correlate the boundaries of the cone and lava flow between it and the radar image (than it was using the topographic map).

TABLE 1
SP MOUNTAIN RANGE-AZIMUTH SCALE CORRECTION FACTORS

Channel	IPL File No.	Pixel Spacing (m)		Scale Multiplication Factor	
		Azimuth	Range	Azimuth	Range
X_{HH}	584-1	1.5	$\frac{1.5}{1.152}$	1	1.152
X_{HV}	585-1	1.5	$\frac{1.5}{1.112}$	1	1.112
L_{HH}	587-1	1.5	$\frac{1.5}{1.308}$	1	1.308
L_{HV}	586-1	1.5	$\frac{1.5}{1.306}$	1	1.306

factors are within 7 percent of those indicated for the original ideal approach. The decision was made that it would not be cost-effective to use eighteen times as much computer time to eliminate an error of this magnitude.

Images which have been both SR-to-GR-corrected and range-azimuth-scale-corrected were produced. Measurements were made on these images in order to determine how closely the desired unity range-azimuth scale ratio was achieved. The results are shown in Table 2. It can be seen that the errors in scale ratio range from 2.1 to 5.9 percent.

2.4 INTENSITY CORRECTION

The intensity of the radar imagery has variations within the image due to (1) radar antenna gain variation, (2) radar range variation, and (3) radar display irregularities. The radar image intensities can be corrected for antenna gain variation by increasing the intensity of image components at each depression angle to the value they would have with peak antenna gain. This is done by multiplying each value by the square of the ratio of peak gain to actual gain. All image components away from the peak gain angle will be increased in intensity.

The radar image intensity variation due to radar range variation can be corrected by a factor

$$\left[\frac{R}{R_c}\right]^{-3}.$$

where R_c is the range to the center of the scene. The received echo from identical targets at different ranges varies as R^{-4}, but the compression factor attained by the synthetic aperture radar processor increases in proportion to R. These two variations with range result in the R^{-3} relationship. Since the center range of the display was chosen as the reference range, the near-range

TABLE 2
SCALE RATIOS ACHIEVED BY CORRECTION PROCESS

IPL Number	Radar Channel	Scale Ratio Achieved
584	X_{HH}	1.027
585	X_{HV}	1.021
587	L_{HH}	1.043
586	L_{HV}	1.059

intensities will be decreased and the far-range intensities will be increased.

Correction for radar signal recorder irregularities is accomplished by use of a calibration curve generated from recordings of standard signals and measurements of the image intensities of these standard signals. All image component intensities are multiplied by the ratio of peak response to the response at the range of interest. This brings all image intensities up to the same efficiency across the radar display.

Correction factors for these three intensity variations were calculated at 1000 ft intervals in slant range across the swath. These are summarized in Tables 3, 4, 5, and 6; the pertinent geometry is illustrated in Figure 7. Accurate interpolation at the far edge of the swath required that correction factors be provided out to 40,000 ft.

With these three intensity corrections, each intensity value can be converted to equivalent radar cross section by use of a calibration chart. This equivalent radar cross section could be useful for point reflectors, such as spheres or corner reflectors. However, extended horizontal surfaces will appear weaker at lower depression angles because the reflected power is inversely proportional to the cosine of the depression angle. This is due to the fact that equal sections of horizontal surfaces intercept less of the illuminating radar signal at smaller depression angles. Thus, the reflected signal from extended targets is less at lower depression angles even though the surface reflectivity is constant.

If different channels of radar imagery are to be compared by ratioing or subtraction, data corrected as described above would provide good results only for point targets. If, however, it is desired to compare imagery of horizontal surfaces, the intensities should be corrected for illumination differences. That is, they should be multiplied by cos θ.

TABLE 3
X_{HH} INTENSITY CORRECTION INFORMATION

Ground Range (ft)	Percent of Display Width	Slant Range (ft)	Depression Angle (Degrees)	ΔG^2 (dB)	$10 \log_{10} \left[\frac{R}{R_c}\right]^{-3}$ (dB)	Δ_{eff} (dB)	Total Error (dB)
6,213	0	16,236*	67.5		-5.75		
8,002	4	17,000	61.92		+5.65		
9,951	10	18,000	56.44		+4.40	-0.2	
11,661	15	19,000	52.14		+3.70	-0.2	
13,229	21	20,000	48.59	-14.5	+3.03	-0.2	-11.67
14,698	26	21,000	45.58	-11.0	+2.39	-0.2	-8.81
16,092	32	22,000	42.99	-9.6	+1.79	-0.1	-6.91
17,434	38	23,000	40.71	-6.7	+1.21	-0.0	-5.49
18,736	43	24,000	38.68	-4.7	+0.65	-0.1	-4.15
20,000	49	25,000	36.87	-2.8	+0.12	-0.6	-3.28
20,294	50	25,236	36.47	-2.5	0.00	-0.8	-3.30
21,232	54	26,000	35.23	-1.7	-0.39	-1.1	-3.19
22,450	60	27,000	33.75	-0.8	-0.88	-1.7	-3.38
23,644	65	28,000	32.39	-0.3	-1.35	-2.4	-4.05
24,821	71	29,000	31.14	-0.08	-1.81	-2.2	-4.09
25,981	76	30,000	30.00	0.0	-2.25	-2.1	-4.35
27,129	82	31,000	28.94	-0.05	-2.68	-2.0	-4.73
28,261	86	32,000	27.95	-0.23	-3.09		
29,393	93	33,000	27.04	-0.53	-3.49		
30,522	99	34,000	26.12	-0.95	-3.88		
30,716	100	34,236	25.98	-1.0	-3.97		
31,623		35,000	25.38	-1.1	-4.25		-6.2
32,726		36,000	24.62	-1.8	-4.63		-7.2
33,823		37,000	23.92	-2.0	-4.99		-7.8
34,914		38,000	23.25	-2.5	-5.33		-8.6
36,000		39,000	22.62	-2.8	-5.67		-9.3
37,081		40,000	22.02	-3.2	-6.00		-10.0

*Near edge.

TABLE 4
X_{HV} INTENSITY CORRECTION INFORMATION

Percent of Display Width	Slant Range (ft)	Depression Angle (Degrees)	ΔG^2 (dB)	$10 \log_{10} \left[\frac{R}{R_c}\right]^{-3}$ (dB)	Δ_{eff} (dB)	Total Error (dB)
0	16,236	67.50	-34.0	5.75	-5.0	-33.3
4	17,000	61.92	-34.0	5.65	-5.0	-33.4
10	18,000	56.44	-23.8	4.40	-5.5	-24.9
15	19,000	52.14	-19.6	3.70	-5.6	-24.5
21	20,000	48.59	-16.8	3.03	-5.9	-19.7
26	21,000	45.58	-14.4	2.39	-6.0	-18.0
32	22,000	42.99	-11.9	1.79	-5.8	-15.9
38	23,000	40.71	-8.9	1.21	-5.4	-13.1
43	24,000	38.68	-5.9	0.65	-5.1	-10.4
49	25,000	36.87	-3.4	0.12	-5.0	-8.3
50	25,236	36.47	-2.9	0.00	-5.0	-7.9
54	26,000	35.23	-2.1	-0.39	-5.0	-7.5
60	27,000	37.75	-0.9	-0.88	-4.8	-6.6
65	28,000	32.39	-0.3	-1.35	-3.9	-2.9
71	29,000	31.14	0.0	-1.81	-3.0	-4.8
76	30,000	30.00	0.0	-2.25	-2.0	-4.3
82	31,000	28.94	-0.0	-2.68	0.0	-2.7
86	32,000	27.95	-0.2	-3.09	0.0	-3.3
93	33,000	27.04	-0.7	-3.49	0.0	-4.2
99	34,000	26.12	-0.9	-3.88	0.0	-4.8
100	34,236	25.98	-1.1	-3.97	0.0	-5.1
	35,000	25.38	-1.5	-4.26		-5.8
	36,000	24.62	-2.3	-4.63		-6.9
	37,000	23.92	-2.6	-4.99		-7.6
	38,000	23.25	-3.4	-5.33		-8.7
	29,000	22.62	-3.9	-5.67		-9.6
	40,000	22.02	-5.1	-6.00		-11.1

TABLE 5
L_{HH} INTENSITY CORRECTION INFORMATION

Percent of Display Width	Slant Range (ft)	Depression Angle (Degrees)	ΔG^2 (dB)	$10 \log_{10} \left[\frac{R}{R_c}\right]^{-3}$ (dB)	Δ_{eff} (dB)	Total Error (dB)
0	16,236	67.50		5.75		
4	17,000	61.92		5.65		
10	18,000	56.44	-3.4	4.40	-1.5	-0.5
15	19,000	52.14	-2.8	3.70	-0.6	-0.3
21	20,000	48.59	-2.1	3.03	0.0	-0.9
26	21,000	45.58	-1.7	2.39	0.0	-0.7
32	22,000	42.99	-1.3	1.79	0.0	-0.5
38	23,000	40.71	-1.1	1.21	0.0	-0.1
43	24,000	38.68	-0.9	0.65	0.0	-0.3
49	25,000	36.87	-0.6	0.12	0.0	-0.5
50	25,236	36.47	-0.5	0.00	0.0	-0.5
54	26,000	35.23	-0.3	-0.39	-0.1	-0.8
60	27,000	37.75	-0.2	-0.88	-0.5	-1.6
65	28,000	32.39	-0.1	-1.35	-1.1	-2.6
71	29,000	31.14	0.0	-1.81	-2.0	-3.8
76	30,000	30.00	0.0	-2.25	-3.0	-5.3
82	31,000	28.94	0.0	-2.68	-4.5	-7.2
86	32,000	27.95	0.0	-3.09		-7.6
93	33,000	27.04	-0.1	-3.49		-7.1
99	34,000	26.12	-0.2	-3.88		-8.6
100	34,236	25.98	-0.2	-3.97		-8.7
	35,000	25.38	-0.4	-4.26		-9.2
	36,000	24.62	-0.4	-4.63		-9.5
	37,000	23.92	-0.5	-4.99		-10.0
	38,000	23.25	-0.6	-5.33		-10.4
	29,000	22.62	-0.7	-5.67		-10.9
	40,000	22.02	-0.8	-6.00		-11.3

TABLE 6
L_{HV} INTENSITY CORRECTION INFORMATION

Percent of Display Width	Slant Range (ft)	Depression Angle (Degrees)	ΔG^2 (dB)	$10 \log_{10} \left[\frac{R}{R_c}\right]^{-3}$ (dB)	Δ_{eff} (dB)	Total Error (dB)
0	16,236	67.50		5.75	-10.0	
4	17,000	61.92		5.65	-10.0	
10	18,000	56.44	-4.9	4.40	-10.0	-10.5
15	19,000	52.14	-3.8	3.70	-9.0	-9.1
21	20,000	48.59	-2.9	3.03	-8.0	-7.9
26	21,000	45.58	-2.4	2.39	-7.0	-7.0
32	22,000	42.99	-1.8	1.79	-6.0	-6.0
38	23,000	40.71	-1.4	1.21	-5.0	-5.2
43	24,000	38.68	-1.1	0.65	-4.0	-4.5
49	25,000	36.87	-0.8	0.12	-2.8	-3.5
50	25,236	36.47	-0.6	0.00	-2.5	-3.1
54	26,000	35.23	-0.5	-0.39	-1.9	-2.8
60	27,000	37.75	-0.4	-0.88	-1.4	-2.7
65	28,000	32.39	-0.2	-1.35	-1.0	-2.6
71	29,000	31.14	0.0	-1.81	-0.8	-2.6
76	30,000	30.00	0.0	-2.25	-0.7	-3.0
82	31,000	28.94	0.0	-2.68	-0.5	-3.2
86	32,000	27.95	0.1	-3.09		-3.7
93	33,000	27.04	-0.2	-3.49		-4.2
99	34,000	26.12	-0.4	-3.88		-4.8
100	34,236	25.98	-0.6	-3.97		-4.9
	35,000	25.38	-0.6	-4.26		-4.9
	36,000	24.62	-0.6	-4.63		-5.2
	37,000	23.92	-0.7	-4.99		-5.7
	38,000	23.25	-0.8	-5.33		-6.1
	29,000	22.62	-0.9	-5.67		-6.6
	40,000	22.02	-1.0	-6.00		-7.0

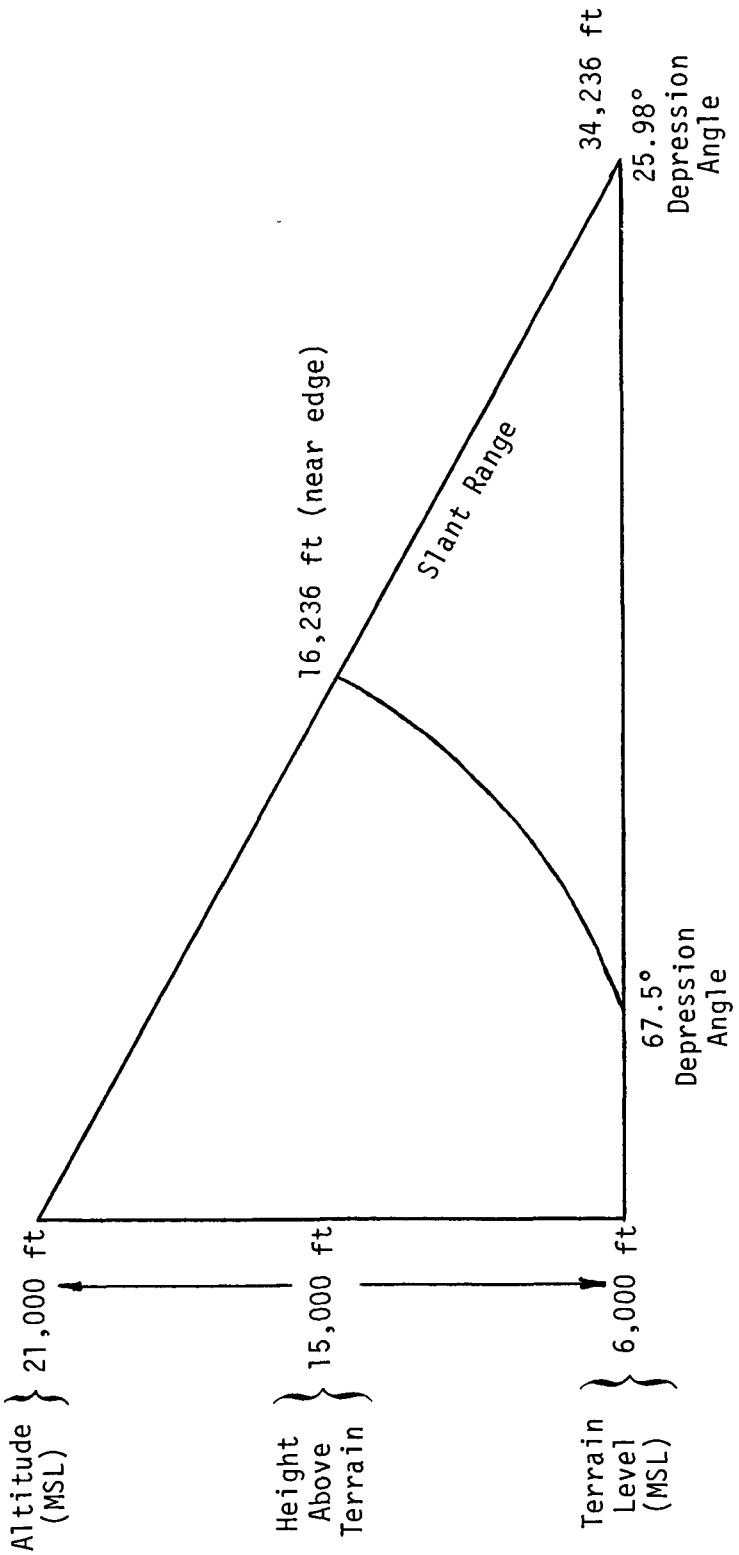

FIGURE 7. DATA-COLLECTION GEOMETRY.

Radar images with all four intensity corrections would appear more uniform over a range of depression angles if the target scene were all horizontal with no relief. However, point target intensities would be distorted. For the purposes of this analysis, all four intensity corrections are considered necessary.

Figures 8, 9, 10, and 11 show the images which have been intensity-corrected (in addition to being SR-to-GR and range-azimuth-scale-corrected). The symbol "GSC" is used to show that all these corrections have been made. Intensity correction is signified by the "C" (for "calibration").

It should be pointed out that these data (as well as all other image data discussed and presented in this report) are amplitude data and not intensity data. If these amplitude data were squared to obtain intensity data, the resulting dynamic range could not be fully represented in digital form because of computer limitations. In order to avoid this loss of information, amplitude data were used in the digital analysis described in the following chapter.

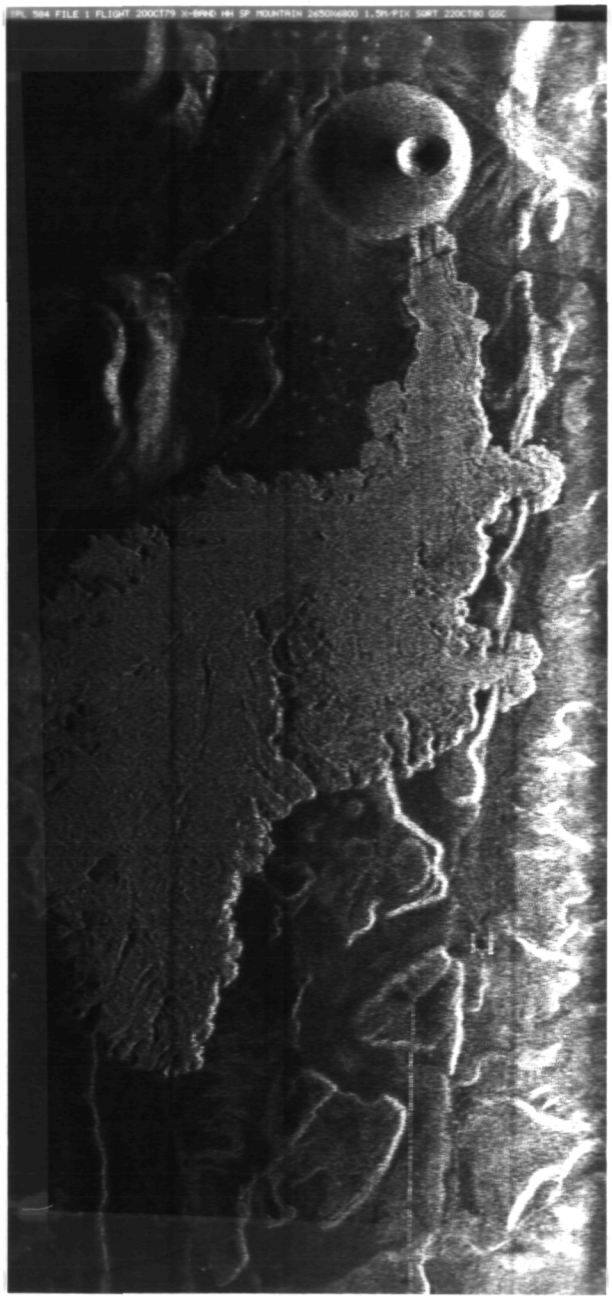

FIGURE 8. X_{HH} ERDC IMAGERY CORRECTED FOR SR-TO-GR, RA.-AZ. SCALE, AND INTENSITY.

1.04-32
.05-5

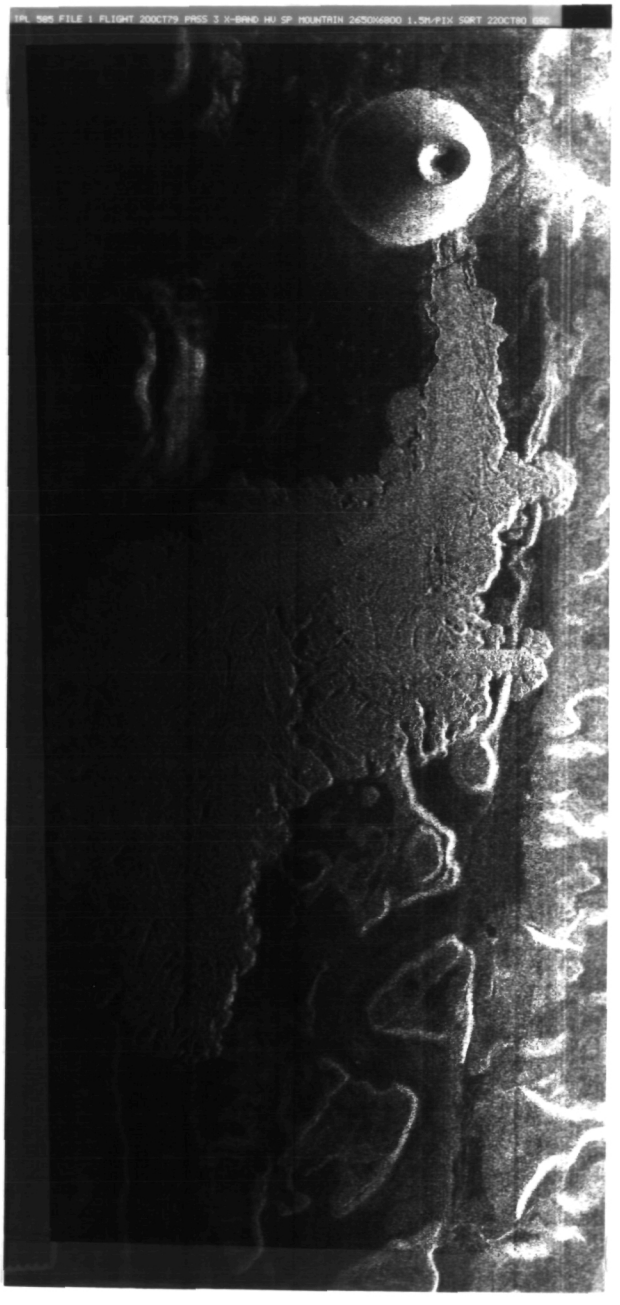

FIGURE 9. X_{HV} ERDC IMAGERY CORRECTED FOR SR-TO-GR, RA.-AZ. SCALE, AND INTENSITY.

.05-80
1-11 - 5

FIGURE 10. L_{HH} ERDC IMAGERY CORRECTED FOR SR-TO-GR, RA.-AZ. SCALE, AND INTENSITY.

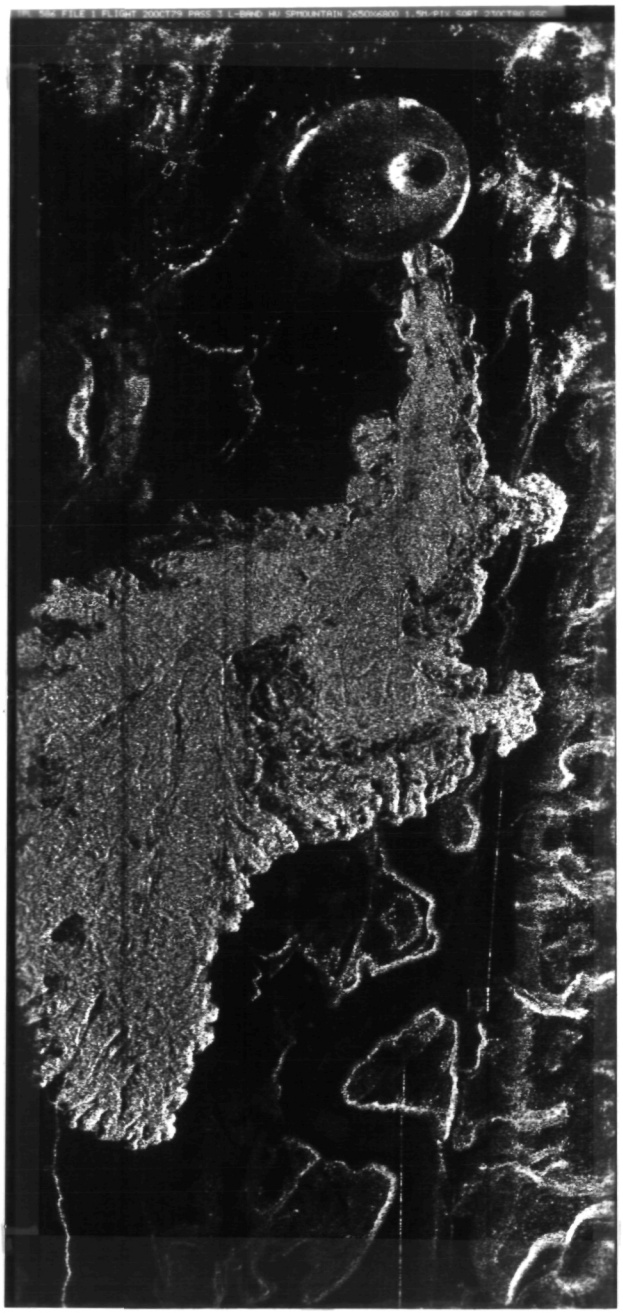

FIGURE 11. L_{HV} ERDC IMAGERY CORRECTED FOR SR-TO-GR, RA.-AZ. SCALE, AND INTENSITY.

1:05-80
1:14-5

3
IMAGE ANALYSIS AND INTERPRETATION

Analysis of the X-L SAR imagery of the SP Mountain area included the visual interpretation of the corrected four-channel SAR data and evaluation of two digital image enhancement techniques. Since the operating wavelengths were 3 cm (X-band) and 23 cm (L-band), different roughness scales should be apparent in the different images. These comparisons are presented in the following section (3.1). Next, image differencing was accomplished to accentuate the differential response in the like- and cross-polarized imagery (Section 3.2). Finally, a method for correction for the ground relief was developed and used to correct for distortion caused by vertical terrain displacement (Section 3.3).

3.1 IMAGERY INTERPRETATION

Interpretation of the SP Mountain SP flow SAR imagery was accomplished with the aid of a Geological Survey map (1962). Two distinct surface units are indicated: unit 1 consists of basaltic blocks and unit 2 corresponds to sand-filled areas with grassy vegetation cover. Some more highly vegetated areas are indicated near the southern fan.

In general, unit 1 and unit 2 do not reflect much differently on the four channels. They are better differentiated at L-band than at X-band, perhaps due to the reflectivity of the grass at X-band. The northern fan is shown as sandy on its northeast portion, but the radar images do not show this. Some of the vegetated areas appear as prominent return areas on all four channels, but they do not appear significantly different from returns from rocks.

Detailed comparison of imagery from the various channels points out specific features with backscatter signatures that change dramatically with changes in polarization or frequency. Referring to Figures 8-11, the following observations can be made:

There is a prominent rectangle east of SP Mountain on L_{HH}, but it's shape is quite different on L_{HV} and it does not show on X_{HH} or X_{HV}.

There is an area of strong return at the base of SP Mountain (ESE) on L_{HH}. This is fairly prominent in L_{HV}, and barely visible on the X-band channels.

There is a low return strip near the base of SP Mountain (N, E, and possibly W) on the L-band channels. This strip is not visible on the X-band channels.

The X-band channels show what may be a road running east and west just north of SP Mountain. This does not show on the L-band channels.

Michilbach tank (NE of the flow) shows on all four channels. The X_{HV} image does not show the fences both east and west of the tank, although they appear on the other three channels.

There are long lines both north and south of Michilbach tank that may be fences. These show brightly at L-band, moderately to weakly at X_{HH}, and cannot be distinguished at X_{HV}.

3.2 DIFFERENCING

One of the ways that two different data channels can be compared is by creating a difference image, in which each pixel is the difference between the corresponding pixels in the two channels being compared. This standard MSS enhancement technique was applied to the L-band HH and HV data channels using the ARIES digital image processing facility. Further information about the digital computer work involved is provided in Appendix B.

The composite difference image in Figure 12 shows L_{HH} components in black and L_{HV} in white. Image components that were equal in both channels would be expected to cancel and appear grey in the

FIGURE 12. DIFFERENCE IMAGERY.

·05-85
·9-1

composite. Image components that are stronger in one channel would be expected to appear in the composite as black or white components, depending upon which channel is stronger. Note that processing streaks in both channels also appear in the composite.

Low return areas in both channels appear as grey areas in the composite. The low-level image texture is less visible in the composite image. The differencing operation has evidently caused the weak areas to cancel to some extent, leaving a nearly featureless grey area.

The moderate and strong components of both channels are all visible but displaced because of poor registration. The rough surface of the lava flow has texture in both channels and in the composite. The shorter-range portion of the lava appears to have more white (cross-polarized) components than black (parallel). This includes the steep near edges of the flow. The far-range portion of the flow has more dark (parallel) components.

The lack of alignment of the two channels is quite noticeable throughout the composite image. Strong components of both channels can be seen (L_{HH} dark and L_{HV} light) with a slight displacement in range. For example, a single point image within the rectangle and another southwest of the rectangle both appear as displaced black and white images. The strong linear images northwest of center can be seen clearly as displaced pairs also. If these pairs were properly registered, they would tend to cancel each other out, rather than appearing prominently. A notable exception is a rectangular array of components in the southeast portion of the image that appears almost exclusively in the cross-polarized channel. It appears white in the composite.

The observed displacement is greater at near range than at far range; this non-uniformity may be due to slightly different sweep speeds in the two channels. Co-registration of SAR channels is therefore probably required, in addition to the slant-to-ground

range and aspect ratio correction (see Section 2.3), to produce a satisfactory composite image. Identical channels could be used with the subtraction routine to test the accuracy of the registration.

Use of the channel subtraction technique does appear to enhance some features of the SP flow and to increase contrast between low and moderate to strong returns. Its effectiveness is significantly degraded, however, by mis-registration of the two channels. This example points out the need for developing algorithms to co-register SAR channels.

3.3 REMOVAL OF RELIEF DISPLACEMENT

In a sidelooking radar (SLAR) image, the slant-range representation causes two basic geometric distortions. The first is the distortion in representing a horizontal terrain segment ("slant-to-ground" distortion). The second is the distortion in representing vertical terrain segments ("relief displacement").

The first kind of distortion is easily removed for flat surfaces, such as oceans and midwest agricultural fields. This correction has been discussed in Section 2.3.1.

Correction of the second type of distortion, however, has not been accomplished to our knowledge. Relief displacement, illustrated in Figure 13, severely distorts SLAR images of mountain and hilly terrain; a relative displacement with elevation occurs toward the ground track of the aircraft. Such a displacement precludes accurate overlays and computer comparison with other imagery such as Landsat, causes "radar foreshortening," and, as shown by the relative positions of A and B in Figure 13, radar "layover." This latter distortion occurs when the downward slope of the terrain toward the aircraft is greater than the perpendicular to the radar beam.

Relief displacement can be removed using topographic data which are available in digital form for the continental United States, and can be obtained from stereo aerial photography elsewhere.

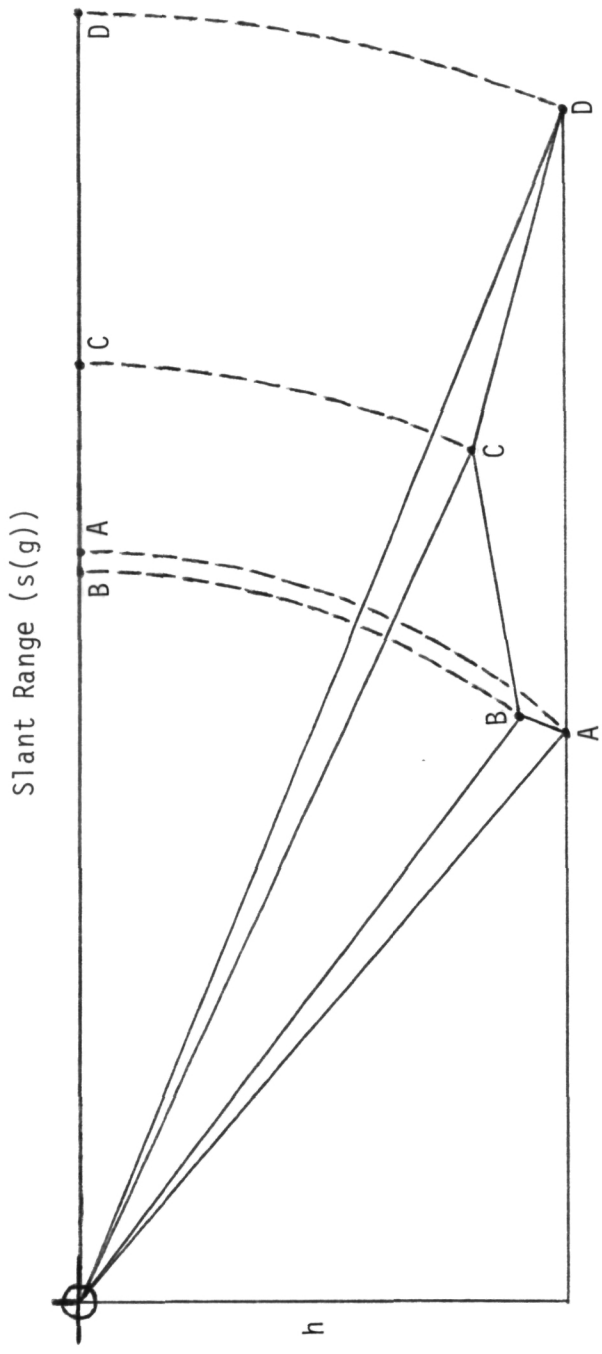

FIGURE 13. RADAR RELIEF DISPLACEMENT.
(In slant range, BA is layover, BC is radar foreshortening. Note that elevation causes relative displacement toward the vehicle.)

If one commences with the map coordinates (ground range) and the flight parameters of the radar, the corresponding slant ranges can easily be found. The image intensity at the corresponding slant range can then be assigned to the proper map coordinate.

The procedure for each ground range sample is as follows:

1. Select a map coordinate (ground range), g, related to the known ground track of the vehicle.

2. Using the known elevation at that coordinate, find the slant range s corresponding to g:

$$s(g) = (g^2 + (h - e)^2)^{1/2}$$

   where e is the elevation and h is the altitude of the aircraft.

3. Assign the image intensity found in the corresponding slant range s(g) to the map coordinate g. As the slant range is discretely sampled, assign the intensity found by nearest neighbor, linear interpolation, or a more sophisticated interpolation as desired or required.

The above procedure is presented in its simplest form. Flight parameter errors, scaling, and bookkeeping difficulties (such as relating digital topographic data skewed with SAR data) will provide sufficient difficulty in execution.

Relief displacement in SAR imagery of SP Mountain in northern Arizona (contours shown in Figure 14) has been removed. SP Mountain is not perfectly rotationally symmetric, but it is close enough to provide a graphic illustration of relief displacement and its removal. The 3-cm (X-band) cross-polarized (HV) imagery is displayed in four manifestations in Figures 2, 15, and 16.

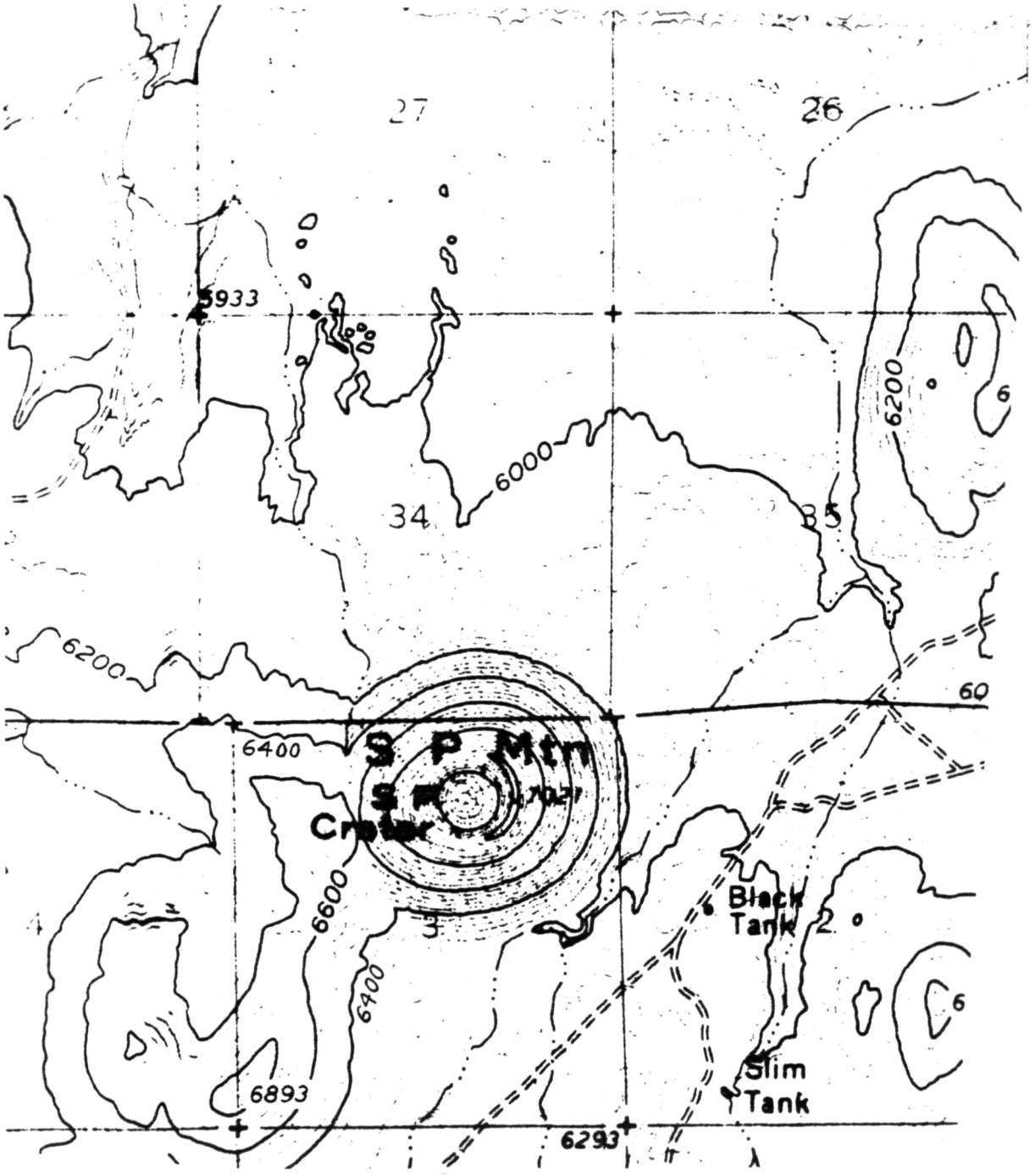

FIGURE 14. TOPOGRAPHIC CONTOURS OF SP MOUNTAIN.

(Note deviations from circular symmetry and higher elevations on west side.)

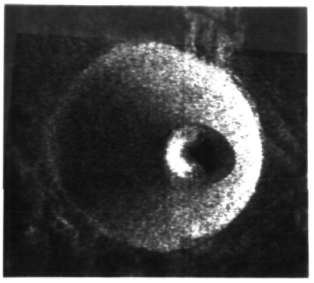

FIGURE 15. SLANT-TO-GROUND-RANGE CONVERSION WITH DATUM PLANE AT TOP OF SP MOUNTAIN.

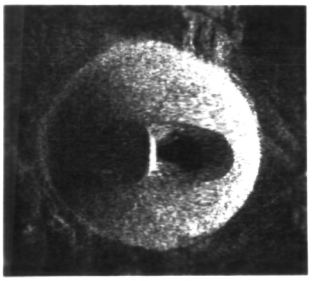

FIGURE 16. REMOVAL OF RELIEF DISPLACEMENT. (Includes slant-to-ground-range conversion.)

.05 - 85
.9 - 1

The slant-range uncorrected imagery shown in Figure 2(a) demonstrates slant-range distortion in that both the base of the mountain and its crater are foreshortened in the range dimension. Relief displacement causes the crater to be imaged unnaturally close to the ground track side of the mountain.

Distortion removal by conventional slant-to-ground range conversion is shown in Figure 2(b), where the datum plane is taken at the base of the mountain. Here, the base of the mountain is rectified to approximate its actual shape (see Figure 14), but the crater is still displaced in position and unnaturally foreshortened.

If the datum plane for conventional slant-to-ground range conversion is taken at the elevation of the crater, the crater's actual shape and position are approximated, but the base of the mountain is distorted and displaced, as shown in Figure 15.

Using the procedure described above, both relief displacement removal and slant-to-ground range conversion are accomplished. The elevation data for SP mountain were approximated by four analytic functions for various sections of the scene. As shown in Figure 16, the preliminary result is less than ideal, but the actual shape of the entire mountain is approximated, with both the shapes of the crater and the base of the mountain closely approximated. Additional effort is required to refine the topographic approximation and develop a more accurate determination of flight parameters.

Thus, a simple procedure for the removal of relief displacement in sidelooking radar imagery has been described and a very preliminary test shown. The procedure requires elevation data and knowledge of flight altitude and ground track. Fortunately, digital elevation data for the continental United States are readily available, and can be obtained elsewhere (with more effort and expense) from stereo aerial photography. The removal of relief displacement will enable accurate overlays of radar imagery upon maps and other types of imagery, such as Landsat.

The computer programs used are discussed in Appendix B.

4
CONCLUSIONS AND RECOMMENDATIONS

4.1 CONCLUSIONS

In carrying out the work discussed in this report, ERIM has demonstrated the use of digital image processing routines that can aid in geological interpretation of SAR imagery. Standard rectification and registration routines have been applied to all four channels of SAR SP mountain data and the resulting imagery has been manually interpreted. In addition an MSS differencing technique for image enhancement has been applied, and an advanced rectification routine for relief displacement has been developed.

Basic preprocessing routines that should be applied previous to interpretation or additional image enhancement include radiometric rectification and image registration. The intensity correction of the data in the range direction has been used in this program to correct for (1) range falloff (R^{-3}), (2) the antenna pattern, and (3) CRT-photo-recorder variations. Intensity variations in corrected imagery correspond to actual variations in radar backscatter.

Image registration is necessary to compare SAR imagery with maps in ground coordinates. These routines are (1) the slant-range-to-ground-range correction and (2) the range-azimuth scale correction. For the latter, a relatively inexpensive approach was employed which permits the modification of the range scale only; this approach gives a unity ratio of range and azimuth scales but does not assure exactly the same image size. If needed in the future, a more sophisticated (and much more expensive) approach is available at ERIM which permits changing both range and azimuth scales; if this approach were used, exact image registration would be possible.

Manual interpretation of the corrected imagery showed that the L-band channels gave a better representation of the general geologic units of the area than did X-band. It was suggested that increased

reflectivity of the vegetation at X-band masked rock (or soil) signature differences. Some vegetated areas showed strong returns on all four channels. Several features showing distinctly different signatures in the various polarization or frequency channels were also observed.

In an attempt to enhance observed polarization differences, an MSS differencing technique was applied to the L-band channels. This technique generates a new image in which each pixel is the difference between the corresponding pixels in the two single channels. Although differencing did enhance the contrast of the scene and make some flow features more prominent, accurate registration of the two channels proved to be a critical factor in the effectiveness of this technique.

Additional image improvement was obtained with a correction for relief displacement. This technique has been developed to remove the effects of range layover so that, for example, the crater at the top of SP mountain is correctly aligned with its actual geographic position. The feasibility of this technique has been demonstrated, but additional refinement of the algorithm is required to obtain completely satisfactory results. Accurate relief displacement correction and registration routines are needed prior to combining SAR imagery with maps or Landsat imagery in a digital format.

4.2 RECOMMENDATIONS

The results of this analysis have provided a valuable basis from which to determine future research projects related to digital image analysis. The following recommendations are direct consequences of this study:

1. Develop improved registration techniques for SAR data channels. The image registration algorithm could be tested by using identical data as inputs to the image differencing algorithm. If the images are in perfect registration, the difference will be zero. Any departure from zero would be a measure of lack of registration.

2. Investigate the application of other MSS image enhancement techniques, such as ratioing, to SAR digital data.

3. Develop an improved relief displacement correction algorithm. This will involve refining the accuracy of the topographic approximation equations and developing a more accurate determination of flight parameters.

4. Develop a technique to register four-channel SAR digital data with Landsat data.

APPENDIX A

DIGITIZATION PARAMETERS

APPENDIX A
DIGITIZATION PARAMETERS

Figures A-1, A-2, A-3, and A-4 show the computer printouts of the digitization parameters for tapes IPL 584, 585, 586, and 587. The CCTs and these printouts were generated by ERIM's Hybrid Image Processing Facility (HIPF).

```
 R BCOMP
*SDSP
SAR DIGITIZING SYSTEM PARAMETERS
CURRENT DATE?22OCT80
FLIGHT DATE, PASS NUMBER, AUX DATA?20OCT79 PASS 3 SF MOUNTAIN
RADAR RANGE SCALE FACTOR, RADAR AZIMUTH SCALE FACTOR
?196700,15000
SIGNAL FILM ASPECT RATIO IS 13.1133
OPTICAL AZIMUTH DEMAGNIFICATION?13.7
DESIRED IMAGE RESOLUTION; RANGE, AZIMUTH:?3,3
SAMPLES PER RANGE RESOLUTION ELEMENT (NYQUIST=2)?2
SAMPLES PER AZIMUTH RESOLUTION ELEMENT (NYQUIST=2)?2
RANGE SCALE FACTOR= 1.5 METERS/PIXEL
AZIMUTH SCALE FACTOR= 1.5 METERS/PIXEL
RANGE IMAGE PIXEL SPACING IS 7.62582 MICRONS
DISSECTOR RELAY LENS MAGNIFICATION?1
RANGE SCAN APERTURE IN RADAR SPACE = 3.5406 METER GAUSSIAN
AZIMUTH IMAGE PIXEL SPACING IS 7.29927 MICRONS
AZIMUTH IMAGE SLIT WIDTH (MICRONS)?5
AZIMUTH SCAN APERTURE IN RADAR SPACE = 1.0275 METER RECT
ALONG TRACK START POSITION (KILOMETERS)?9.5
RANGE OFFSET TO START POINT (KILOMETERS)?1.3
NUMBER OF PIXELS PER LINE, NUMBER OF LINES, POINT SKIP
?2650,6800,0
SWATH WIDTH IS 3.975 KILOMETERS
ALONG TRACK LENGTH IS 10.2 KILOMETERS
START POINT 175
STOP POINT 2825
LASER WAVELENGTH (NANOMETERS?515
FREQUENCY PLANE WEIGHTING FILTER?NO
RANGE FREQUENCY PLANE APERTURE IS 18.9094 MILLIMETERS
AZIMUTH FREQUENCY PLANE APERTURE IS 1.442 MILLIMETERS
DEFLECTION VOLTAGE AT FULL SCAN (3600) IS 2.05623 VOLTS
DEFLECTION VOLTAGE AT STOP POINT IS 1.29738 VOLTS
LASER POWER (MW), OBJECTIVE FL (MM), MULTIPLIER VOLTAGE, GAIN
?400,8,1800,5
CONVERSION MODE (LINEAR OR SQRT)?SQRT
INTEGRATION TIME (MICROSECONDS)?990
SIGNAL FILM RUN LENGTH IS 680 MILLIMETERS
SIGNAL FILM DRIVE FREQUENCY IS 388.683 HERTZ
FILM DRIVE SIGNAL PERIOD IS 2572.79 MICROSECONDS
TIME PER LINE IS 2.76086 SECONDS
RUN TIME IS 312 MINUTES
FEET OF RECORDING TAPE REQUIRED = 2302
 1792.93  4553.31

 R BCOMP
GO
LABEL?IPL 584 FILE 1 FLIGHT 20OCT79 X-BAND HH SF MOUNTAIN 2650X6800 1.5M/PIX SQRT 22OCT80
LINES?6800
GO
EOF
 TOTAL      7 BAD LINES
```

FIGURE A-1. HIPF PARAMETER PRINTOUT FOR CCT NO. IPL-584.

```
 R BCOMP
*SDSP
SAR DIGITIZING SYSTEM PARAMETERS
CURRENT DATE?22OCT80
FLIGHT DATE, PASS NUMBER, AUX DATA?20OCT79 PASS 3 SP MOUNTAIN
RADAR RANGE SCALE FACTOR, RADAR AZIMUTH SCALE FACTOR
?195200,15000
SIGNAL FILM ASPECT RATIO IS 13.0133
OPTICAL AZIMUTH DEMAGNIFICATION?13.7
DESIRED IMAGE RESOLUTION; RANGE, AZIMUTH:?3,3
SAMPLES PER RANGE RESOLUTION ELEMENT (NYQUIST=2)?2
SAMPLES PER AZIMUTH RESOLUTION ELEMENT (NYQUIST=2)?2
RANGE SCALE FACTOR= 1.5 METERS/PIXEL
AZIMUTH SCALE FACTOR= 1.5 METERS/PIXEL
RANGE IMAGE PIXEL SPACING IS 7.68442 MICRONS
DISSECTOR RELAY LENS MAGNIFICATION?1
RANGE SCAN APERTURE IN RADAR SPACE = 3.5136 METER GAUSSIAN
AZIMUTH IMAGE PIXEL SPACING IS 7.29927 MICRONS
AZIMUTH IMAGE SLIT WIDTH (MICRONS)?5
AZIMUTH SCAN APERTURE IN RADAR SPACE = 1.0275 METER RECT
ALONG TRACK START POSITION (KILOMETERS)?9.5
RANGE OFFSET TO START POINT (KILOMETERS)?1.3
NUMBER OF PIXELS PER LINE, NUMBER OF LINES, POINT SKIP
?2650,6800,0
SWATH WIDTH IS 3.975 KILOMETERS
ALONG TRACK LENGTH IS 10.2 KILOMETERS
START POINT 175
STOP POINT 2825
LASER WAVELENGTH (NANOMETERS?515
FREQUENCY PLANE WEIGHTING FILTER?NO
RANGE FREQUENCY PLANE APERTURE IS 18.7652 MILLIMETERS
AZIMUTH FREQUENCY PLANE APERTURE IS 1.442 MILLIMETERS
DEFLECTION VOLTAGE AT FULL SCAN (3600) IS 2.07203 VOLTS
DEFLECTION VOLTAGE AT STOP POINT IS 1.30735 VOLTS
LASER POWER (MW), OBJECTIVE FL (MM), MULTIPLIER VOLTAGE, GAIN
?400,8,1800,5
CONVERSION MODE (LINEAR OR SQRT)?SQRT
INTEGRATION TIME (MICROSECONDS)?990
SIGNAL FILM RUN LENGTH IS 680 MILLIMETERS
SIGNAL FILM DRIVE FREQUENCY IS 388.683 HERTZ
FILM DRIVE SIGNAL PERIOD IS 2572.79 MICROSECONDS
TIME PER LINE IS 2.76086 SECONDS
RUN TIME IS 312 MINUTES
FEET OF RECORDING TAPE REQUIRED = 2302
 1792.93  4553.31

*R DISS3
DG
LABEL?IPL 585 FILE 1 FLIGHT 20OCT79 PASS 3 X-BAND HV SP MOUNTAIN 2650X6800 1.5M/FIX SQRT 22OCT80
LINES?6800
GO?GO
 STOP
27041 TOTAL      1 P.D.T.
EOF

  NO ATTEN
EOF

  NO ATTEN
```

FIGURE A-2. HIPF PARAMETER PRINTOUT FOR CCT NO. IPL-585.

```
 R BCOMP
#SDSP
SAR DIGITIZING SYSTEM PARAMETERS
CURRENT DATE?23OCT80
FLIGHT DATE, PASS NUMBER, AUX DATA?200CT79 PASS 3 SF MOUNTAIN
RADAR RANGE SCALE FACTOR, RADAR AZIMUTH SCALE FACTOR
?185465,41500
SIGNAL FILM ASPECT RATIO IS 4.46904
OPTICAL AZIMUTH DEMAGNIFICATION?13.7
DESIRED IMAGE RESOLUTION; RANGE, AZIMUTH:?3,3
SAMPLES PER RANGE RESOLUTION ELEMENT (NYQUIST=2)?2
SAMPLES PER AZIMUTH RESOLUTION ELEMENT (NYQUIST=2)?2
RANGE SCALE FACTOR= 1.5 METERS/PIXEL
AZIMUTH SCALE FACTOR= 1.5 METERS/PIXEL
RANGE IMAGE PIXEL SPACING IS 8.08778 MICRONS
DISSECTOR RELAY LENS MAGNIFICATION?1
RANGE SCAN APERTURE IN RADAR SPACE = 3.33837 METER GAUSSIAN
AZIMUTH IMAGE PIXEL SPACING IS 2.63829 MICRONS
AZIMUTH IMAGE SLIT WIDTH (MICRONS)?5
AZIMUTH SCAN APERTURE IN RADAR SPACE = 2.84275 METER RECT
ALONG TRACK START POSITION (KILOMETERS)?9.5
RANGE OFFSET TO START POINT (KILOMETERS)?1.3
NUMBER OF PIXELS PER LINE, NUMBER OF LINES, POINT SKIP
?2650,6800,0
SWATH WIDTH IS 3.975 KILOMETERS
ALONG TRACK LENGTH IS 10.2 KILOMETERS
START POINT 175
STOP POINT 2825
LASER WAVELENGTH (NANOMETERS?515
FREQUENCY PLANE WEIGHTING FILTER?NO
RANGE FREQUENCY PLANE APERTURE IS 17.8294 MILLIMETERS
AZIMUTH FREQUENCY PLANE APERTURE IS 3.98953 MILLIMETERS
DEFLECTION VOLTAGE AT FULL SCAN (360O) IS 2.18079 VOLTS
DEFLECTION VOLTAGE AT STOP POINT IS 1.37597 VOLTS
LASER POWER (MW), OBJECTIVE FL (MM), MULTIPLIER VOLTAGE, GAIN
?400,8,1800,5
CONVERSION MODE (LINEAR OR SQRT)?SQRT
INTEGRATION TIME (MICROSECONDS)?990
SIGNAL FILM RUN LENGTH IS 245.783 MILLIMETERS
SIGNAL FILM DRIVE FREQUENCY IS 140.488 HERTZ
FILM DRIVE SIGNAL PERIOD IS 7118.05 MICROSECONDS
TIME PER LINE IS 2.76086 SECONDS
RUN TIME IS 312 MINUTES
FEET OF RECORDING TAPE REQUIRED = 2300
 3230.49 -34995.6

.R DISS3
DG
LABEL?IPL 586 FILE 1 FLIGHT 200CT79 PASS 3 L-BAND HV SFMOUNTAIN 2650X6800 1.5M PIX SQRT 230CT80
LINES?6800
GO?GO
 STOP
27041 TOTAL       4 BAD LINES
EOF

  NEXT?RE
BOF

  NEXT?
```

FIGURE A-3. HIPF PARAMETER PRINTOUT FOR CCT NO. IPL-586.

```
 R BCOMP
*SDSP
SAR DIGITIZING SYSTEM PARAMETERS
CURRENT DATE?24OCT80
FLIGHT DATE, PASS NUMBER, AUX DATA?,20OCT79 PASS 3 L MOUNTAIN
RADAR RANGE SCALE FACTOR, RADAR [illegible]
?185465,41500
SIGNAL FILM ASPECT RATIO IS 4.[illegible]
OPTICAL AZIMUTH DEMAGNIFICATION=15.
DESIRED IMAGE RESOLUTION; RANGE, AZIMUTH [illegible]
SAMPLES PER RANGE RESOLUTION ELEMENT (NYQUIST 2)?2
SAMPLES PER AZIMUTH RESOLUTION ELEMENT (NYQUIST 2)?2
RANGE SCALE FACTOR= 1.5 METERS/PIXEL
AZIMUTH SCALE FACTOR= 1.5 METERS/PIXEL
RANGE IMAGE PIXEL SPACING IS 3.08778 MICRONS
DISSECTOR RELAY LENS MAGNIFICATION?1
RANGE SCAN APERTURE IN RADAR SPACE = 3.33837 METER GAUSSIAN
AZIMUTH IMAGE PIXEL SPACING IS 2.63829 MICRONS
AZIMUTH IMAGE SLIT WIDTH (MICRONS)?5
AZIMUTH SCAN APERTURE IN RADAR SPACE = 2.84275 METER RECT
ALONG TRACK START POSITION (KILOMETERS)?9.5
RANGE OFFSET TO START POINT (KILOMETERS)?1.3
NUMBER OF PIXELS PER LINE, NUMBER OF LINES, POINT SKIP
?2650,6800,0
SWATH WIDTH IS 3.975 KILOMETERS
ALONG TRACK LENGTH IS 10.2 KILOMETERS
START POINT 175
STOP POINT 2825
LASER WAVELENGTH (NANOMETERS?515
FREQUENCY PLANE WEIGHTING FILTER?NO
RANGE FREQUENCY PLANE APERTURE IS 17.8294 MILLIMETERS
AZIMUTH FREQUENCY PLANE APERTURE IS 3.98953 MILLIMETERS
DEFLECTION VOLTAGE AT FULL SCAN (3600) IS 2.18079 VOLTS
DEFLECTION VOLTAGE AT STOP POINT IS 1.37597 VOLTS
LASER POWER (MW), OBJECTIVE FL (MM), MULTIPLIER VOLTAGE, GAIN
?400,8,1800,5
CONVERSION MODE (LINEAR OR SQRT)?SQRT
INTEGRATION TIME (MICROSECONDS)?220
SIGNAL FILM RUN LENGTH IS 245.793 MILLIMETERS
SIGNAL FILM DRIVE FREQUENCY IS 140.[illegible] HERTZ
FILM DRIVE SIGNAL PERIOD IS 7119.05 MICROSECONDS
TIME PER LINE IS 2.76086 SECONDS
RUN TIME IS 312 MINUTES
FEET OF RECORDING TAPE REQUIRED = 2302
 3230.49 -34995.6

.R DISS3
DG
LABEL?IPL 587 FILE 1 FLIGHT 20OCT79 PASS 3 L-BAND HH SF MOUNTAIN 2650X6800 1.5M/PIX SAR: 24OCT80
LINES?6800
GO?GO
 STOP
27041 TOTAL      2 BAD LINES
EOF
```

FIGURE A-4. HIPF PARAMETER PRINTOUT FOR CCT NO. IPL-587.

APPENDIX B

DIGITAL COMPUTER WORK

APPENDIX B
DIGITAL COMPUTER WORK

B.1 INTRODUCTION

The following image data for four channels in the slant-range plane were provided:

X Band HH Polarization - Tape IPL 584
X Band HV Polarization - Tape IPL 585
L Band HV Polarization - Tape IPL 586
L Band HH Polarization - Tape IPL 587

These data were supplied in byte form and the image sizes (no. of records x no. of elem./rec.) are given in Table B-1.

TABLE B-1
IMAGE SIZES

Image	Size
IPL 584	6800 x 2650
IPL 585	6800 x 3000
IPL 586	6800 x 3000
IPL 587	6800 x 3000

B.2 IMAGE RE-SCALING

B.2.1 FIRST APPROACH

The first part of this task requires re-scaling of the images, both in range and azimuth.

The software available for this operation in the ARIES facility is a re-sampling algorithm under UIC[141,21] and task name DSMPRD. This program requires complex-word data as input and a program* was written to reformat the image data.

*UIC[144,21] Task RTOC.

The size of the newly-formatted data is a huge 81.6 x 10^6 bytes, and even in a large disk, it is difficult to find space for a contiguous file of this size. Consequently, the complex-valued formatted data was generated in three sections.

Input data buffer size in the present PDP 11/45 system is restricted to a maximum 2048 complex words in the re-sampling program (DSMPRD). Accordingly, each record must be processed in two sections.

In conclusion, this procedure requires six program runs for each channel.

B.2.2 SECOND APPROACH

The procedure above is very time-consuming and it does not seem to be cost-effective. The azimuth scale change requirement was therefore dropped and the range scale factor was adjusted to maintain the same aspect ratio.

The scale change (in the range direction) can now be accomplished with a program designed to convert data from the slant-range plane to the ground-range plane with a range scale change capability. This software is implemented in the ARIES facility in UIC[150,033] under the task name STG.

The histograms corresponding to the four tapes generated are shown in Figures B-1, B-2, B-3, and B-4.

B.3 INTENSITY CALIBRATION

The purpose of the calibration is to affect the radar data by the antenna polar pattern and the recorder transfer function multiplicative corrections in order to obtain an accurate measurement of the terrain reflectivity at a particular wavelength and polarization.

REAL HISTOGRAM
E(X**4) = 9825256.
E(X**2) = 2045.403
F(X) = 40.14580
SQRT(X)) = 6.130463
MAX. MAG. OF ELEM. = 255.0000
NO. OF PIXELS = 21488000

VALUE	%	CUM %	0 10 20 30 40 50 60 ● 70 80 90 100
0.00	0.60	0.60	>****
8.00	6.90	7.51	>**********
16.00	14.90	22.41	>**********
24.00	16.41	38.81	>**********
32.00	16.16	54.97	>**********
40.00	14.43	69.40	>**********
48.00	11.02	80.42	>**********
56.00	7.50	87.91	>**********
64.00	4.58	92.49	>**********
72.00	2.88	95.37	>**********
80.00	1.76	97.14	>**********
88.00	1.09	98.23	>********
96.00	0.65	98.88	>****
104.00	0.40	99.28	>**
112.00	0.25	99.53	>**
120.00	0.16	99.69	>*
128.00	0.10	99.79	>*
136.00	0.06	99.86	>
144.00	0.04	99.90	>
152.00	0.03	99.93	>
160.00	0.02	99.95	>
168.00	0.01	99.96	>
176.00	0.01	99.97	>
184.00	0.01	99.98	>
192.00	0.01	99.99	>
200.00	0.00	99.99	>
208.00	0.00	99.99	>
216.00	0.00	100.00	>
224.00	0.00	100.00	>
232.00	0.00	100.00	>
240.00	0.00	100.00	>
248.00	0.00	100.00	>
256.00	0.00	100.00	>
264.00	0.00	100.00	>
272.00	0.00	100.00	>
280.00	0.00	100.00	>
VALUE	%	CUM %	0 10 20 30 40 50 60 70 80 90 100

FIGURE B-1. HISTOGRAM FOR TAPE IPL-584 GS (X_{HH}).

REAL HISTOGRAM
E(X**4) = 5388982.
E(X**2) = 521.3749
E(X) = 18.63874
E(SQRT(X)) = 4.177984
MAX. MAG. OF ELEM. = 255.0000
NO. OF PIXELS = 21488000

VALUE	%	CUM %	0 10 20 30 40 50 60 70 80 90 100
0.00	2.32	2.32	>*****
8.00	44.97	47.29	>**********
16.00	32.95	80.24	>**********
24.00	12.32	92.56	>**********
32.00	4.09	96.65	>*********
40.00	1.62	98.27	>****
48.00	0.70	98.97	>**
56.00	0.35	99.31	>*
64.00	0.17	99.48	>
72.00	0.09	99.58	>
80.00	0.05	99.63	>
88.00	0.03	99.66	>
96.00	0.02	99.68	>
104.00	0.08	99.76	>
112.00	0.01	99.77	>
120.00	0.00	99.77	>
128.00	0.00	99.77	>
136.00	0.00	99.78	>
144.00	0.00	99.78	>
152.00	0.00	99.78	>
160.00	0.00	99.78	>
168.00	0.00	99.78	>
176.00	0.07	99.85	>
184.00	0.00	99.85	>
192.00	0.00	99.85	>
200.00	0.00	99.85	>
208.00	0.00	99.85	>
216.00	0.07	99.93	>
224.00	0.00	99.93	>
232.00	0.07	100.00	>
240.00	0.00	100.00	>
248.00	0.00	100.00	>
256.00	0.00	100.00	>
264.00	0.00	100.00	>
272.00	0.00	100.00	>
280.00	0.00	100.00	>
VALUE	%	CUM %	0 10 20 30 40 50 60 70 80 90 100

FIGURE B-2. HISTOGRAM FOR TAPE IPL-585 GS (X_{HV}).

REAL HISTOGRAM
E(X**4) = 7755532.
E(X**2) = 1569.607
E(X) = 34.80600
E(SQRT(X)) = 5.723655
MAX. MAG. OF ELEM. = 251.0000
NO. OF PIXELS = 21488000

VALUE	%	CUM %	0 10 20 30 40 50 60 70 80 90 100
0.00	0.01	0.01	>
8.00	5.61	5.62	>**********
16.00	24.88	30.49	>**********
24.00	24.37	54.86	>**********
32.00	15.35	70.21	>**********
40.00	10.81	81.02	>**********
48.00	7.11	88.13	>**********
56.00	4.49	92.63	>**********
64.00	2.62	95.25	>**********
72.00	1.69	96.94	>*******
80.00	1.08	98.02	>****
88.00	0.68	98.70	>***
96.00	0.42	99.12	>**
104.00	0.28	99.40	>*
112.00	0.19	99.58	>*
120.00	0.12	99.70	>
128.00	0.08	99.77	>
136.00	0.05	99.83	>
144.00	0.04	99.87	>
152.00	0.03	99.90	>
160.00	0.02	99.92	>
168.00	0.02	99.93	>
176.00	0.01	99.95	>
184.00	0.01	99.96	>
192.00	0.01	99.96	>
200.00	0.01	99.97	>
208.00	0.00	99.97	>
216.00	0.00	99.98	>
224.00	0.00	99.98	>
232.00	0.01	99.99	>
240.00	0.01	100.00	>
248.00	0.00	100.00	>
256.00	0.00	100.00	>
264.00	0.00	100.00	>
272.00	0.00	100.00	>
280.00	0.00	100.00	>
VALUE	%	CUM %	0 10 20 30 40 50 60 70 80 90 100

FIGURE B-3. HISTOGRAM FOR TAPE IPL-587 GS (L_{HH}).

REAL HISTOGRAM
E(X**4) = 0.4810484E+08
E(X**2) = 3875.079
E(X) = 52.45364
E(SQRT(X)) = 6.935626
MAX. MAG. OF ELEM. = 252.0000
NO. OF PIXELS = 21488000

VALUE	%	CUM %	0 10 20 30 40 50 60 70 80 90 100
0.00	0.00	0.00	>
8.00	0.90	0.90	>*****
16.00	12.51	13.41	>**********
24.00	19.48	32.89	>**********
32.00	14.12	47.02	>**********
40.00	10.39	57.40	>********
48.00	8.11	65.51	>******
56.00	6.64	72.15	>*****
64.00	5.29	77.44	>****
72.00	4.60	82.04	>****
80.00	3.89	85.93	>***
88.00	3.14	89.07	>***
96.00	2.51	91.57	>**
104.00	2.02	93.59	>**
112.00	1.60	95.19	>*
120.00	1.14	96.33	>*
128.00	0.83	97.15	>*
136.00	0.64	97.80	>*
144.00	0.51	98.30	>*
152.00	0.38	98.68	>*
160.00	0.29	98.97	>*
168.00	0.23	99.20	>*
176.00	0.18	99.38	>*
184.00	0.13	99.51	>*
192.00	0.10	99.61	>*
200.00	0.08	99.68	>
208.00	0.06	99.74	>
216.00	0.05	99.79	>
224.00	0.04	99.83	>
232.00	0.05	99.89	>
240.00	0.11	100.00	>*
248.00	0.00	100.00	>
256.00	0.00	100.00	>
264.00	0.00	100.00	>
272.00	0.00	100.00	>
280.00	0.00	100.00	>
VALUE	%	CUM %	0 10 20 30 40 50 60 70 80 90 100

FIGURE B-4. HISTOGRAM FOR TAPE IPL-586 GS (L_{HV}).

This calibration can be implemented in the slant-range plane (preferably) or in the ground-range plane. This latter implementation should be affected by any possible scale changes previously applied.

In the ARIES facility, a software package* was implemented that reads a small number of samples of the calibration vector, fits a polynomial function to these data (least-squares criterion), and evaluates the calibration vector components for all range locations.

The histograms corresponding to the four tapes generated are shown in Figures B-5, B-6, B-7, and B-8.

B.4 IMAGE DIFFERENCE

The image difference between the L-band HH and HV channels was obtained. This difference was obtained pixel-by-pixel according to the expression

$$DIF = IM1 - IM2(E1/E2) + BIAS,$$

where E1 and E2 are the average values of image 1 and image 2, respectively. A bias was used to allow an accurate representation of the bipolar nature of the image.

Given the slightly different scales of image 1 and image 2, the difference obtained is not totally accurate and thus is enhanced along edge-type features.

Two software packages were implemented in the ARIES facility to obtain the image difference. A slow Fortran task [144,21]INDIF.TSK and a fast AP120B based [144,21]IMDIF.APP were used. Both read two disk-based images in byte form and generated to disk a byte-form image difference. See Figure B-9.

Figure B-10 shows the histogram for the difference image data.

*UIC[144,21] Tasks Read and Inter.

REAL HISTOGRAM
E(X**4) = 837981.8
E(X**2) = 517.6817
E(X) = 19.33797
E(SQRT(X)) = 4.208871
MAX. MAG. OF ELEM. = 182.0000
NO. OF PIXELS = 21488000

VALUE	%	CUM %	0 10 20 30 40 50 60 70 80 90 100
0.00	10.35	10.35	>**********
8.00	35.87	46.22	>**********
16.00	25.16	71.38	>**********
24.00	14.63	86.01	>**********
32.00	7.51	93.52	>**********
40.00	3.49	97.01	>**********
48.00	1.57	98.59	>****
56.00	0.73	99.32	>**
64.00	0.34	99.66	>*
72.00	0.16	99.82	>
80.00	0.08	99.90	>
88.00	0.04	99.95	>
96.00	0.02	99.97	>
104.00	0.01	99.98	>
112.00	0.01	99.99	>
120.00	0.00	99.99	>
128.00	0.00	100.00	>
136.00	0.00	100.00	>
144.00	0.00	100.00	>
152.00	0.00	100.00	>
160.00	0.00	100.00	>
168.00	0.00	100.00	>
176.00	0.00	100.00	>
184.00	0.00	100.00	>
192.00	0.00	100.00	>
200.00	0.00	100.00	>
208.00	0.00	100.00	>
216.00	0.00	100.00	>
224.00	0.00	100.00	>
232.00	0.00	100.00	>
240.00	0.00	100.00	>
248.00	0.00	100.00	>
256.00	0.00	100.00	>
264.00	0.00	100.00	>
272.00	0.00	100.00	>
280.00	0.00	100.00	>
VALUE	%	CUM %	0 10 20 30 40 50 60 70 80 90 100

FIGURE B-5. HISTOGRAM FOR TAPE IPL-584 GSC (X_{HH}).

REAL HISTOGRAM
E(X**4) = 273269.2
E(X**2) = 75.73699
E(X) = 6.025203
E(SQRT(X)) = 2.260968
MAX. MAG. OF ELEM. = 205.0000
NO. OF PIXELS = 21488000

VALUE	%	CUM %	0 10 20 30 40 50 60 70 80 90 100
0.00	72.89	72.89	>**********
8.00	21.76	94.65	>**********
16.00	3.99	98.64	>*****
24.00	0.78	99.42	>*
32.00	0.30	99.72	>
40.00	0.11	99.83	>
48.00	0.05	99.87	>
56.00	0.03	99.90	>
64.00	0.02	99.92	>
72.00	0.01	99.93	>
80.00	0.01	99.94	>
88.00	0.01	99.95	>
96.00	0.01	99.96	>
104.00	0.01	99.96	>
112.00	0.01	99.97	>
120.00	0.01	99.97	>
128.00	0.00	99.98	>
136.00	0.00	99.98	>
144.00	0.00	99.98	>
152.00	0.00	99.99	>
160.00	0.00	99.99	>
168.00	0.00	99.99	>
176.00	0.00	100.00	>
184.00	0.00	100.00	>
192.00	0.00	100.00	>
200.00	0.00	100.00	>
208.00	0.00	100.00	>
216.00	0.00	100.00	>
224.00	0.00	100.00	>
232.00	0.00	100.00	>
240.00	0.00	100.00	>
248.00	0.00	100.00	>
256.00	0.00	100.00	>
264.00	0.00	100.00	>
272.00	0.00	100.00	>
280.00	0.00	100.00	>

FIGURE B-6. HISTOGRAM FOR TAPE IPL-585 GSC (X_{HV}).

REAL HISTOGRAM
E(X**4) = 456410.2
E(X**2) = 405.7859
E(X) = 17.69262
E(SQRT(X)) = 4.076658
MAX. MAG. OF ELEM. = 158.0000
NO. OF PIXELS = 21488000

VALUE	%	CUM %	0 10 20 30 40 50 60 70 80 90 100
0.00	4.52	4.52	>*********
8.00	48.36	52.88	>**
16.00	26.14	79.02	>**************************
24.00	12.00	91.03	>************
32.00	5.34	96.36	>***********
40.00	2.20	98.57	>*****
48.00	0.84	99.41	>**
56.00	0.33	99.74	>*
64.00	0.14	99.88	>
72.00	0.06	99.94	>
80.00	0.03	99.97	>
88.00	0.02	99.99	>
96.00	0.01	100.00	>
104.00	0.00	100.00	>
112.00	0.00	100.00	>
120.00	0.00	100.00	>
128.00	0.00	100.00	>
136.00	0.00	100.00	>
144.00	0.00	100.00	>
152.00	0.00	100.00	>
160.00	0.00	100.00	>
168.00	0.00	100.00	>
176.00	0.00	100.00	>
184.00	0.00	100.00	>
192.00	0.00	100.00	>
200.00	0.00	100.00	>
208.00	0.00	100.00	>
216.00	0.00	100.00	>
224.00	0.00	100.00	>
232.00	0.00	100.00	>
240.00	0.00	100.00	>
248.00	0.00	100.00	>
256.00	0.00	100.00	>
264.00	0.00	100.00	>
272.00	0.00	100.00	>
280.00	0.00	100.00	>
VALUE	%	CUM %	0 10 20 30 40 50 60 70 80 90 100

FIGURE B-7. HISTOGRAM FOR TAPE IPL-587 GSC (L_{HH}).

REAL HISTOGRAM
E(X**4) = 8780161.
E(X**2) = 1603.363
E(X) = 33.58832
E(SQRT(X)) = 5.541334
MAX. MAG. OF ELEM. = 230.0000
NO. OF PIXELS = 21488000

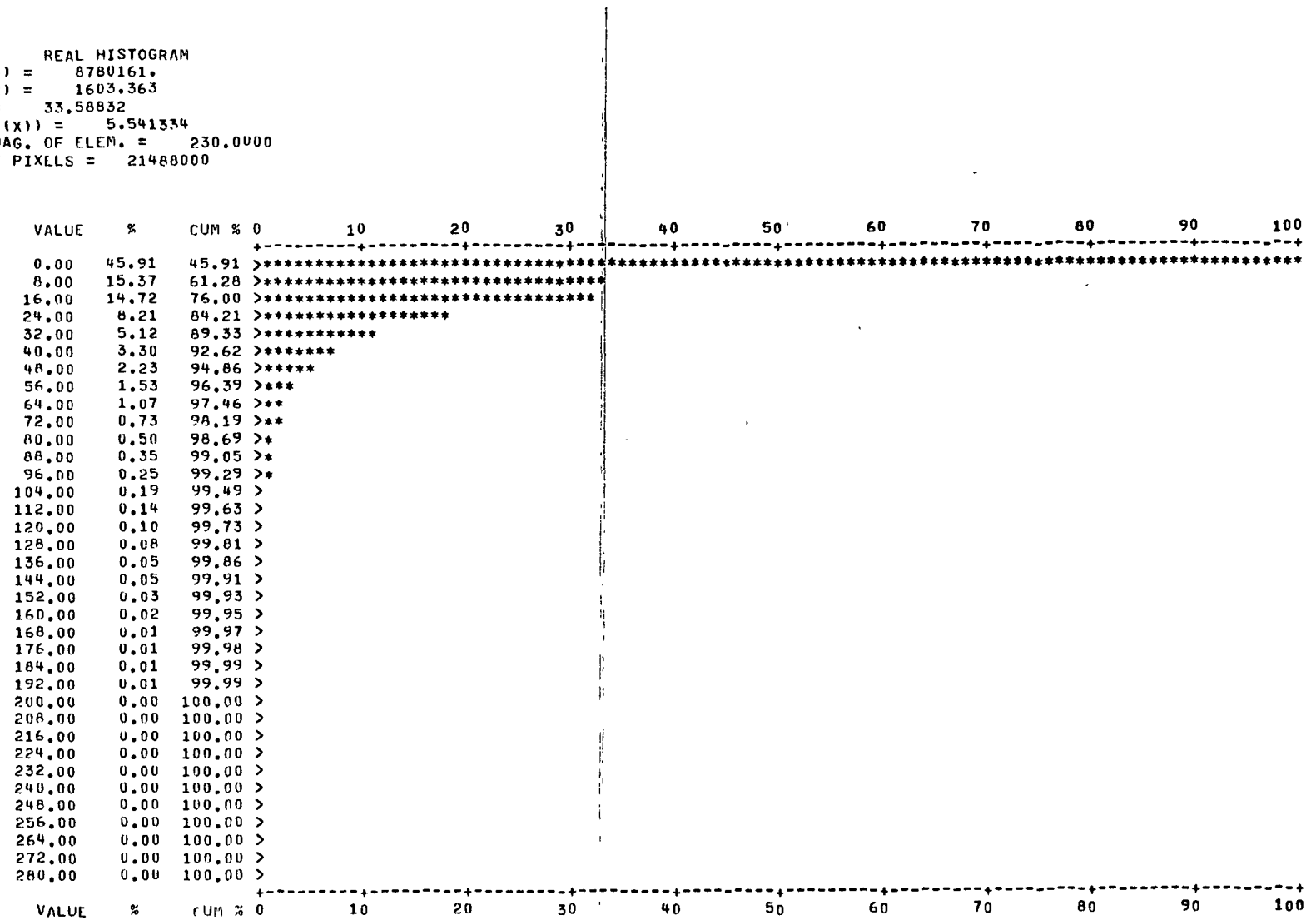

VALUE	%	CUM %
0.00	45.91	45.91
8.00	15.37	61.28
16.00	14.72	76.00
24.00	8.21	84.21
32.00	5.12	89.33
40.00	3.30	92.62
48.00	2.23	94.86
56.00	1.53	96.39
64.00	1.07	97.46
72.00	0.73	98.19
80.00	0.50	98.69
88.00	0.35	99.05
96.00	0.25	99.29
104.00	0.19	99.49
112.00	0.14	99.63
120.00	0.10	99.73
128.00	0.08	99.81
136.00	0.05	99.86
144.00	0.05	99.91
152.00	0.03	99.93
160.00	0.02	99.95
168.00	0.01	99.97
176.00	0.01	99.98
184.00	0.01	99.99
192.00	0.01	99.99
200.00	0.00	100.00
208.00	0.00	100.00
216.00	0.00	100.00
224.00	0.00	100.00
232.00	0.00	100.00
240.00	0.00	100.00
248.00	0.00	100.00
256.00	0.00	100.00
264.00	0.00	100.00
272.00	0.00	100.00
280.00	0.00	100.00

FIGURE B-8. HISTOGRAM FOR TAPE IPL-586 GSC (L_{HV}).

```
;
;
;       PROGRAM TO ACE DIFFERENCE
;
;
;       RUN AS - IMDIF.APP
;
;
;
;
;
APC VCLR 0,1,65536
SETAPSTORE/FILE=LP1:[144,21]IDF.G/NAPE=1560/NAPL=1/NEAPL=1560-
/I*2/RSTRT=6800/APLOC=0,0
APTOCK/NEW
;
ECHOOFF
;
;
;
APD MOD L=0,4,1 DATA=256,0,255,1.698,50
;
LET A=1
;
;
LABEL LOOP
;
OKTOAP/FILE=LP1:[144,21]IPL587.GSC/NOE=3160/NOL=10/RSTRT=A-
/BYTE/UNSI/APLOC=0,10
;
OKTOAP/FILE=LP1:[144,21]IPL586.GSC/NOE=3160/NOL=10/RSTRT=A-
/BYTE/UNSI/APLOC=0,31610
;
;
;
APC VSMSB/PAR=10,1,3,31610,1,10,1,3160/REP=10/INC=3160,0,0,3160,0,3160,0,0
APC VSADD/PAR=10,1,4,10,1,3160/REP=10/INC=3160,0,0,3160,0,0
;
;
;
APC VCLIP 10,1,1,2,10,1,31600
APC VFIX 10,1,10,1,31600
;
;
APC VFLT 10,1,10,1,31600
APC VSMA 10,2,0,11,2,11,2,15800
APC VFIX 11,2,11,1,15800
;
;
;
APTOCK/OLD/NAPL=10/RSTRT=A/APLOC=0,11
LET A=A+10
IF (A>6800)GOTO END
GOTO LOOP
LABEL END
;
;
```

FIGURE B-9. IMAGE DIFFERENCE PROGRAM.

```
          REAL HISTOGRAM
E(X**4) =    0.1420643E+08
E(X**2) =     2965.828
E(X) =     50.63776
E(SQRT(X)) =     6.875089
MAX. MAG. OF ELEM. =     255.0000
NO. OF PIXELS =    21408000

   VALUE      %      CUM %  0         10        20        30        40        50        60        70        80        90        100
                            +---------+---------+---------+---------+---------+---------+---------+---------+---------+---------+
    0.00     4.22     4.22  >*******************
    8.00     2.09     6.31  >*********
   16.00     3.24     9.54  >***************
   24.00     5.12    14.66  >************************
   32.00     8.42    23.09  >****************************************
   40.00    14.62    37.71  >*********************************************************************
   48.00    22.01    59.72  >*****************************************************************************************************
   56.00    19.49    79.21  >*********************************************************************************************
   64.00     9.94    89.15  >*********************************************
   72.00     4.93    94.08  >**********************
   80.00     2.71    96.79  >************
   88.00     1.34    98.13  >******
   96.00     0.74    98.87  >***
  104.00     0.44    99.30  >**
  112.00     0.26    99.56  >*
  120.00     0.16    99.72  >*
  128.00     0.10    99.82  >
  136.00     0.06    99.88  >
  144.00     0.04    99.91  >
  152.00     0.02    99.94  >
  160.00     0.02    99.96  >
  168.00     0.01    99.97  >
  176.00     0.01    99.98  >
  184.00     0.01    99.98  >
  192.00     0.01    99.99  >
  200.00     0.00    99.99  >
  208.00     0.00   100.00  >
  216.00     0.00   100.00  >
  224.00     0.00   100.00  >
  232.00     0.00   100.00  >
  240.00     0.00   100.00  >
  248.00     0.00   100.00  >
  256.00     0.00   100.00  >
  264.00     0.00   100.00  >
  272.00     0.00   100.00  >
  280.00     0.00   100.00  >
                            +---------+---------+---------+---------+---------+---------+---------+---------+---------+---------+
   VALUE      %      CUM %  0         10        20        30        40        50        60        70        80        90        100
```

FIGURE B-10. HISTOGRAM FOR IMAGE DIFFERENCE DATA.

B.5 CORRECTION OF RELIEF DISPLACEMENT

The implementation of the algorithm to remove relief displacement from the SP Mountain Data was carried out and its feasibility was shown. The elevation model utilized is, necessarily, inaccurate and this is the reason for the less-than-perfect reconstruction.

The ARIES software developed and used for this purpose is the following:

1. [144,21]CONTOUR.TSK - A Fortran program modeling the elevation map of SP Mountain. See Figure B-11.

2. [144,21]TNSTOG.TSK - A Fortran program that reads disk-based slant-range image data and a disk-based elevation map and then reconstructs a ground-range map with elevation correction. This particular program does not achieve a unity aspect ratio. This is due to the fact that (normally) the sample spacing is the same in range and azimuth for the slant-range data. Upon SR-to-GR conversion, the ground-range data sample spacing changes and, to a first-order approximation, it is assumed constant along the range of interest. A second display program would be required to achieve unity aspect ratio. Given the initial stage of this idea, an approximate unity aspect ratio was obtained using a simple technique. See Figure B-12.

Figures B-13 and B-14 show the histograms for the relief displacement correction data. Figure B-13 corresponds to the SR-to-GR correction while Figure B-14 corresponds to the complete correction.

```
C
C
C
C       PROGRAM CONTOUR.FTN
C
C
C
C
      INTEGER*2 C(1000)
C
C
C
C
      INTEGER*2 CTRL1(64),ERR(6)
      BYTE FNAME1(32)
C
C
C
      PI=3.141592654
      TPI=2*PI
      PI2=PI/2
C
C
      WRITE(2,2)
2     FORMAT('ENTER # OF RECORDS #OF ELEMENTS/RECORD :')
      READ(1,3)NIL,NE
3     FORMAT(2I5)
C
C
      ICRE=1
      WRITE(2,4)
4     FORMAT('ENTER FILE NAME :')
      CALL FILMAN(FNAME1,4,0,ICRE,NE,NIL,CTRL1,1)
C
C
C
      DO 1000 J=1,NIL
C
C
      IF(J-50*(J/50).NE.0)GO TO 6
      WRITE(2,7)J
6     CONTINUE
7     FORMAT(I5)
C
C
C
C
C
C
C
C       THIS PROGRAM COMPUTES THE ELEVATIONS ON SP MOUNTAIN
C       CORRESPONDING TO SAMPLES OF SAR DATA.
C
C       A = ELEVATION OF APEX OF SP MOUNTAIN (IMAGINARY POINT
C           ABOVE CRATER)
C       S = SLOPE OF SIDES OF SP MOUNTAIN
C       DR = SAMPLING INTERVAL IN RANGE
C       DA = SAMPLING INTERVAL IN AZIMUTH
C       E(I) = ELEVATION FUNCTION
C       IA,JA = APEX RANGE AND AZIMUTH INDEXES
```

FIGURE B-11. PROGRAM CONTOUR FOR RELIEF DISPLACEMENT CORRECTION.

```
C       R = CRATER RADIUS
C       HR = HORIZONTAL DISTANCE FROM APEX TO HIGHEST
C            POINT AT SOUTHEAST EDGE OF CRATER
C       HHR = HORIZONTAL DISTANCE FROM APEX TO 6200 FT
C             ELEVATION
C       I,J = RANGE AND AZIMUTH INDEXES
C       A = VIEW ANGLE AT WHICH ELEVATION IS 6200 FT
C       B = S ANGLE AT WHICH ELEVATION IS 6200 FT
C
        DATA A,S,DR,DA,IA,JA//267.52,0.556,7.4507,4.9212,480,588/
        DATA B,HR,HHR,G,P/630.0,1358.824,1920.0,0.838,-2.705/
C
C
C
C
C
        DO 50 I=1,ME
C
C
C
C       FIND DISTANCE DOWN SLOPE FROM APEX
C
C
        DIST=SQRT(((IA-I)*DR)**2+((JA-J)*DA)**2)
C
C       FIND VERTICAL DISTANCE FROM APEX
C
        VDIST=S*DIST
C
C
C
C
C       TEST FOR POINTS INSIDE CRATER
C
C
        IF(DIST.LT.R)GO TO 10
C
C
C
C       FIND ANGLE OF LOCATION FROM APEX
C
C
        X=FLOAT(IA-I)
        Y=FLOAT(JA-J)
        ANGLE=ATAN2(X,Y)
        IF(ANGLE.LT.G.OR.ANGLE.GT.B)GO TO 20
C
C
C
C
C
C       FIND THE ELEVATIONS ON THE EAST SIDE:
C
C
        R=R+TPI
        IF(ANGLE.LT.0)ANGLE=ANGLE+TPI
C
        GGG=400.*SIN(PI*(R-ANGLE)/(R-G))
        IF(VDIST.LT.A-GGG)GO TO 30
        ELEV=6200.+GGG
        E(I)=FLOAT(ELEV)
```

FIGURE B-11. PROGRAM CONTOUR FOR RELIEF DISPLACEMENT CORRECTION. (Continued)

```
            GO TO 50
      C
      C
      C
      C     FIND ELEVATIONS IN CENTRAL CRATER
      C
      C
      10    WH=S*P
            ELEV=A-VH-SQRT(R**2-DIST**2)
            E(I)=NINT(ELEV)
            GO TO 50
      20    IF(DIST.GT.RRR)GO TO 40
      30    ELEV=A-VDIST
            E(I)=NINT(ELEV)
            GO TO 50
      40    ELEV=6200.
            E(I)=NINT(ELEV)
      50    CONTINUE
      C
      C
            JOUT=0
            CALL WRITE(CTRL1,ERR(5),E,NE,JOUT)
            CALL IOWAIT(CTRL1,ERR(6))
      C
      C
      1000  CONTINUE
      C
      C
      C
            CALL DETACH(CTRL1,IERR)
      C
      C
      C
            END
      C
      C
      C
      C
```

FIGURE B-11. PROGRAM CONTOUR FOR RELIEF DISPLACEMENT CORRECTION. (Concluded)

```
C
C
C
C       PROGRAM TNSTOGE.FTN
C
C
C
C       NIL,NIE=NO. OF INPUT RANGE LINES, ELEMENTS.
C
C
      INTEGER*2 SP(1000),GP(1000),SHADO(1000)
      INTEGER*2 CTRL1(61),CTRL2(61),ERR(8)
      INTEGER*2 CTRL3(61)
      BYTE FNAME1(32),FNAME2(32)
      BYTE FNAME3(32)
      INTEGER*2 E(1000)
C
C
C
      WRITE(2,10)
10    FORMAT('$ENTER # OF RECORDS, # OF ELEMENTS/RECORD: ')
      READ(1,20)NIL,NIE
20    FORMAT(2I5)
      WRITE(2,21)
21    FORMAT('$ENTER AIRCRAFT ALTITUDE AND REFERENCE GROUND LEVEL: ')
      READ(1,22)ALT,GAV
22    FORMAT(2F16.8)
C
C
      WRITE(2,30)
30    FORMAT('$ENTER INPUT FILE: ')
      CALL FILNAM(FNAME1,3,1,0,NIE,NIL,CTRL1,1)
C
C
      WRITE(2,35)
35    FORMAT('$ENTER FIRST RECORD, LAST RECORD: ')
      READ(1,36)INIT,LAST
36    FORMAT(2I5)
C
C
C
      ICRE=1
      WRITE(2,40)
40    FORMAT('$ENTER OUTPUT FILE: ')
      CALL FILNAM(FNAME2,4,0,ICRE,NIE,NIL,CTRL2,1)
      WRITE(2,41)
41    FORMAT('$ENTER ELEVATION DATA FILE: ')
      CALL FILNAM(FNAME3,5,1,0,NIE,NIL,CTRL3,1)
C
C
C
      DATA DS,SRIS,P/4.9212,22080.0525,630.0/
      DATA IA,JA/400,588/
C
C
C
C
      GRIS=SQRT(SRIS**2-(ALT-GAV)**2)
      DG=SQRT((SRIS+DS)**2-(ALT-GAV)**2)-GRIS
C
```

FIGURE B-12. PROGRAM TNSTOGE FOR RELIEF DISPLACEMENT CORRECTION.

```
C
C
C
C
C       ------------------------
C       SLANT TO RANGE CONVERSION
C       ------------------------
C
C
C
C
C
        DO 1000 J=INIT,LAST
C
C
        IF(J-50*(J/50).NE.0)GO TO 46
        WRITE(2,45)J
45      FORMAT(I5)
46      CONTINUE
C
C
C
C
C
        JIN=J
        CALL READ(CTRL3,ERR(2),E,NIE,JIN)
        CALL IOWAIT(CTRL3,ERR(4))
C
                JIN=J
                CALL READ(CTRL1,ERR(2),SR,NIE,JIN)
                CALL IOWAIT(CTRL1,ERR(4))
C
C
C
C
C
                DO 50 I=1,NIE
C
                        GR(I)=0
50                      SHADO(I)=1
C
C
C
C
C               FIND SLANT RANGE WHICH CORRESPONDS TO
C                 GIVEN GROUND RANGE.
C
C
                DO 80 I=1,NIE
                IF(SHADO(I).EQ.0) GO TO 80
                TOTRAN=SQRT((GRIS+(I-1)*DG)**2+(ALT-E(I))**2)
                II=NINT((TOTRAN-SRIS)/DS)
                IF(II.GT.NIE.OR.II.LT.1) GO TO 80
                GR(I)=SR(II)
80              CONTINUE
C
C
C
C
                JOUT=J
                CALL WRITE(CTRL2,ERR(5),GR,NIE,JOUT)
                CALL IOWAIT(CTRL2,ERR(6))
```

FIGURE B-12. PROGRAM TNSTOGE FOR RELIEF DISPLACEMENT CORRECTION. (Continued)

```
C
C
C
C
C
1000    CONTINUE
C
C
C
C
C
        CALL DETACH(CTRL1,IERR)
        CALL DETACH(CTRL2,IERR)
        CALL DETACH(CTRL3,IERR)
C
C
C
        END
C
```

FIGURE B-12. PROGRAM TNSTOGE FOR RELIEF DISPLACEMENT CORRECTION. (Concluded)

REAL HISTOGRAM
E(X**4) = 2461588.
E(X**2) = 736.9459
E(X) = 21.08660
E(SQRT(X)) = 4.305494
MAX. MAG. OF FLEM. = 201.0000
NO. OF PIXELS = 645920

VALUE	%	CUM %	0 10 20 30 40 50 60 70 80 90 100
0.00	9.27	9.27	>******************************
8.00	25.94	35.21	>**
16.00	33.63	68.84	>**
24.00	14.71	83.55	>***
32.00	5.97	89.53	>*******************
40.00	3.60	93.13	>***********
48.00	2.36	95.49	>*******
56.00	1.60	97.08	>*****
64.00	1.01	98.10	>***
72.00	0.65	98.75	>**
80.00	0.44	99.19	>*
88.00	0.30	99.49	>*
96.00	0.20	99.69	>*
104.00	0.11	99.80	>
112.00	0.08	99.88	>
120.00	0.05	99.93	>
128.00	0.03	99.96	>
136.00	0.01	99.97	>
144.00	0.01	99.98	>
152.00	0.01	99.99	>
160.00	0.00	99.99	>
168.00	0.00	100.00	>
176.00	0.00	100.00	>
184.00	0.00	100.00	>
192.00	0.00	100.00	>
200.00	0.00	100.00	>
208.00	0.00	100.00	>
216.00	0.00	100.00	>
224.00	0.00	100.00	>
232.00	0.00	100.00	>
240.00	0.00	100.00	>
248.00	0.00	100.00	>
256.00	0.00	100.00	>
264.00	0.00	100.00	>
272.00	0.00	100.00	>
280.00	0.00	100.00	>
VALUE	%	CUM %	0 10 20 30 40 50 60 70 80 90 100

FIGURE B-13. HISTOGRAM FOR SR-TO-GR CORRECTION DATA.

REAL HISTOGRAM
E(X**4) = 2383181.
E(X**2) = 747.6668
E(X) = 22.13653
E(SQRT(X)) = 4.330471
MAX. MAG. OF FLEM. = 201.0000
NO. OF PIXELS = 645920

VALUE	%	CUM %	0 10 20 30 40 50 60 70 80 90 100
0.00	9.27	9.27	>******************************
8.00	25.62	34.89	>**
16.00	32.72	67.60	>**
24.00	14.85	82.45	>**
32.00	6.43	88.88	>*********************
40.00	3.99	92.87	>************
48.00	2.59	95.46	>********
56.00	1.69	97.15	>*****
64.00	1.04	98.19	>***
72.00	0.65	98.84	>**
80.00	0.43	99.26	>*
88.00	0.29	99.55	>*
96.00	0.18	99.73	>*
104.00	0.10	99.83	>
112.00	0.07	99.90	>
120.00	0.04	99.94	>
128.00	0.03	99.97	>
136.00	0.01	99.98	>
144.00	0.01	99.99	>
152.00	0.01	99.99	>
160.00	0.00	100.00	>
168.00	0.00	100.00	>
176.00	0.00	100.00	>
184.00	0.00	100.00	>
192.00	0.00	100.00	>
200.00	0.00	100.00	>
208.00	0.00	100.00	>
216.00	0.00	100.00	>
224.00	0.00	100.00	>
232.00	0.00	100.00	>
240.00	0.00	100.00	>
248.00	0.00	100.00	>
256.00	0.00	100.00	>
264.00	0.00	100.00	>
272.00	0.00	100.00	>
280.00	0.00	100.00	>
VALUE	%	CUM %	0 10 20 30 40 50 60 70 80 90 100

FIGURE B-14. HISTOGRAM FOR SR-TO-GR AND RELIEF DISPLACEMENT CORRECTION DATA.